Analysis and Interpretation of Acidic Nature of Aluminosilicates

Naonobu Katada

Division of Applied Chemistry, Graduate School of Sustainability Science, Tottori University

4-101 Koyama-cho Minami, Tottori 680-8552, Japan

katada@chem.tottori-u.ac.jp

Abstract

Aluminosilicate solid acid catalysts, especially zeolites, have been widely utilized in petroleum refinery and environmentally benign chemical processes. The acidic property of aluminosilicates has been a subject of advanced studies. Recently an ammonia IRMS-TPD (infrared / mass spectroscopy temperature-programmed desorption) method, an application of operando technique, has been developed to quantify the number and strength distribution of each of Brønsted and Lewis sites on a solid. With an aid of quantum chemistry, relationships among the composition, structure and acidic property are being unveiled to totally understand the chemistry of SiOHAl unit in the aluminosilicates.

Key words: Acidic property, Aluminosilicate, Zeolite, Ammonia IRMS-TPD

1. Importance of analysis of solid acidity

Nowadays, we recognize that Brønsted and Lewis acids are different concepts, although they show similar behaviors. The similarity had confused the interpretation of acid base chemistry until 1920's, when Brønsted [1], Lowry [2], Lewis [3] and other researchers discussed and established the definition of acid and base. A number of literatures published in this period evidencing the presence of serious discussion tell us that practical importance of acid base chemistry had already been recognized in this period. It is supposed that they did not discuss on the definition of materials which changed the color of a specific moss, but they discussed for proper understanding of a series

of materials which showed important function such as catalysis.

After 100 years, we still have similar discussion on solid surfaces. Throughout the petroleum era, solid acid catalysts, mainly zeolites and other aluminosilicates, have been utilized in many processes such as fluid catalytic cracking (FCC) [4-6], hydrocracking / hydrotreatment [7] and skeletal isomerization [8] in petroleum refinery (Figure 1) [9,10]. Mainly later than 1980, replacement of liquid acid catalysts with solid acid catalysts realized various environmentally benign chemical processes [11-13], e.g., alkylation-dealkylation of mono-cyclic aromatic compounds [14-18], hydration [19], amination of alcohols [20,21] and phenol [22], Chichibabin condensation [23], and Beckmann rearrangement [24]. Many of materials are now called solid acids, and they are industrially important due to their usage of catalysts, but the type of acid sites, Brønsted or Lewis, or, in some cases, even the presence of acid sites is unclear. However, many kinds of materials are called solid acids, because they show catalytic functions like those of acidic ion exchange resins and H-form zeolites, in which the protons have been clarified to act as Brønsted acid sites. Even on zeolites, relationships among the composition, structure and acidic property have been subjects of serious discussion for finding principles controlling the nature and role of acid sites [25].

To solve energy and environmental problems, development of efficient solid acid catalysts is strongly demanded. The catalysis of solid acid is fundamentally owing to the chemical action of acid sites, in many cases Brønsted acid sites, and therefore it should be necessary to investigate the acidic properties of solid acid catalysts especially aluminosilicates.

In addition, the aluminosilicates, especially zeolites, are utilized as catalyst supports of transition metals and ion exchangers. These functions are also generated by ion exchange ability of aluminosilicates, which may be related with the Brønsted acidic property in their proton forms [26]. Degree of stabilization and electronic nature of transition metal species in atomic dimension held by the ion exchange site are related with the Brønsted acid strength in the H-form of zeolite [27,28]. Such mono-atomically dispersed metal species shows chemical function which is never seen on bulk materials [29].

From these backgrounds, we believe that the analysis of Brønsted acidic property is an important subject. One distinct feature of zeolites is microporosity, and most of commercial amorphous silica alumina catalysts are mesoporous. Therefore, identification of the effects of porosity and acidic property is necessary for fundamental understanding of the catalysis. Nowadays, the analysis of porous nature has been established, but the analysis of acidic properties of solids have been under development. This short review as a proceeding of the plenary lecture in Acid-Base Catalysis 8 describes advances in the measurements and interpretation of acidic properties of zeolites giving new insights on relationships among the composition, structure and acidic property.

2. Advances in measurements of acidic properties of solids

The acidic property of a solid is described by the number (amount), strength and type (Brønsted or Lewis) of acid sites on it. According to the definition by Brønsted, the strength of Brønsted acid site on a solid surface should be shown by some parameters describing the position of equilibrium of the following reaction, i.e., protonation of a probe base:

$$\text{H-A} + \text{B (g)} \rightarrow \text{BH}^{+}\cdots\text{A}^{-} \qquad (1)$$

where H-A is the discussed Brønsted acid site, and B (g) is vapor of probe base. Similarly, the strength of Lewis acid site should be shown by those of the following reaction, i.e., coordination of a probe base [13]:

$$\text{L} + :\text{B (g)} \rightarrow \text{B:L} \qquad (2)$$

where L shows the Lewis acidic species, and ":" shows a pair of electron. As the parameters, equilibrium constant and standard Gibbs energy at a specific temperature such as 298 K, or, a set of standard enthalpy (reaction heat) and standard entropy can be used.

Table 1 lists methods typically used for the measurements of acidic properties of solids. They are classified into [i] titration-based techniques to mainly quantify the number and strength of acid sites such as indicator and ammonia temperature-programmed desorption (TPD) methods, including H/D exchange [30], and [ii] spectroscopy-based techniques to mainly identify Brønsted and Lewis acid sites such as infrared spectroscopy (IR) of adsorbed pyridine and carbon monoxide. By combining these two principles, Niwa et al. developed a method of ammonia infrared / mass spectroscopy temperature-programmed desorption (IRMS-TPD) [31]. It is noteworthy that the IR measurement of adsorbed pyridine can give a way of quantification of the Brønsted and Lewis acid sites on the assumption that the molar extinction coefficient is constant as proposed by Emeis [32].

It should be noted that, apart from the techniques, amines like ammonia and pyridine are protonated by the Brønsted acid site and chemically coordinate to Lewis acid site giving parameters related to the equilibrium, whereas such molecules as argon, carbon monoxide and nitrile are physically adsorbed by acid site. On the other hand, again apart from usually employed techniques, it has been known that pyridine can change the structure (and hence nature) of the solid surface due to its high basicity [33]. Ammonia should have similar nature based on its basicity, although the extent seems low. In addition, ammonia can reduce the transition metal species, if they are present on the surface, resulting in unexpected modification of the property of solid surface. We should use these probe molecules with deep understanding of these advantages and disadvantages.

A typical operando equipment [34] is used for the ammonia IRMS-TPD method. The sample is compressed into a thin wafer and placed in a sample holder. It is fixed in a cell, in which the IR beam passes through calcium fluoride windows and the center of sample wafer. The cell is connected to a vacuum line to which necessary gases can be supplied, and the outlet is connected to vacuum pumps and a mass spectrometer (MS). After a suitable pretreatment, reference IR spectra of the solid sample are repeatedly recorded in a time interval with heating the holder and sample in a carrier gas flow (usually helium) from a temperature lower than the temperature for ammonia adsorption shown below up to a high temperature such as 773 K where all ammonia will be desorbed.

Here, the gas is removed by a vacuum pump from the outlet through a needle valve, giving a certain total pressure in the cell. Then, ammonia is adsorbed by introducing gaseous ammonia into the cell at a relatively low temperature such as 343 K. Subsequently, the sample is again heated at the ramp rate and flow rate of the carrier gas same as those in the measurements of reference IR spectra before the ammonia adsorption. Here IR spectra of sample adsorbing ammonia are recorded, as well as MS at some mass to valence ratios (*m*/*e*) such as 4, 16, 17, 18, 28, 32 and 44 for monitoring the concentrations of carrier gas (helium), desorbed ammonia and unexpected but possible compounds (water, nitrogen, oxygen and carbon dioxide) in the gas phase. A set of the ramp rate, flow rate of carrier gas and the total pressure affect (i) the temperature distribution in the sample wafer, (ii) the signal to noise ratio in mass spectrum (MS) and (iii) the time for transporting the gas from the sample to MS, and all of them influence the accuracy. We recommend 0.033 K s^{-1}, 82 μ mol s^{-1} and 6 kPa for the ramp rate, flow rate of carrier gas and total pressure, respectively. At the last of experiments, standard mixture of ammonia and helium with a known concentration is fed to calibrate the MS detector for absolute quantification [34].

Because a very small amount of solid sample, ca. 10 mg, is employed to form a 1 cm diameter-wafer with sufficient transparency to IR beam, the amount of measured ammonia is small compared to the conventional ammonia TPD typically using 100 mg of the sample. It gives weak intensity of MS signal. The experimental parameters are more strictly limited in the above values than those for the conventional ammonia TPD. The advance in mass spectroscopy was required to perform this kind of measurement. Recently we have developed an automatic analyzer which brought not only the automatization of measurements but also high stability of the sample position, flow rate etc. contributed to improve the accuracy of this method.

The MS gives a desorption profile (called MS-TPD) as shown by the black line in Figure 2. Typical H-form zeolite [35] shows two peaks at low and high temperatures, named *l*- and *h*-peak, respectively. The intensity of *l*-peak is sensitively dependent on the measurement conditions. Due to the small amount of solid sample in IRMS-TPD method compared to the conventional ammonia

TPD, the intensity of *l*-peak is often small or negligible. Usually, the *l*-peak is due to ammonia hydrogen-bonded to cations including NH_4^+ [36-39] and therefore should be ignored in the analysis of acidic property. However, sometimes it is due to ammonia species adsorbed on weak acid site, and therefore, it must not be ignored. In conclusion, we cannot identify the desorption peaks to be considered or ignored with only the information from MS.

Detection of physically adsorbed or hydrogen bonded ammonia species as a desorption peak was pointed out to be a disadvantage of the ammonia TPD method [40]. Introduction of water vapor after the adsorption of ammonia [37,41] or the desorption of ammonia in a humid carrier gas [42] were reported to remove the physically adsorbed and hydrogen bonded species, while the ammonia species adsorbed on the acid site was not affected; water has high boiling point and highly polar O-H bond, contributing to strong physical adsorption and hydrogen bond, respectively, compared to ammonia, while the basicity of water is weaker than ammonia. The introduction of water vapor is therefore utilized as a method to remove unnecessary adsorbed species selectively from the TPD profile, but the disadvantage of this method has been pointed out. In some cases, the co-presence of ammonia and water, probably giving strongly basic conditions, may decompose the framework structure of solid, as reported [43,44]. It should be mentioned that the following phenomena were reported when water vapor was introduced after the adsorption of ammonia on solid acids. Woolery et al. interpreted that ammonia coordinated to Lewis acid sites on zeolite, due to extra-framework Al or framework-anchored Al, was selectively replaced by water [42]. Bagnasco [41] and Naito et al. [45] found that ammonia coordinated to the Lewis acid sites on basic oxide surfaces were replaced by water. Water changed the nature of surface through hydration to weaken the acidity of surface, resulting in no adsorption of ammonia. In conclusion, the introduction of water vapor requires careful consideration not to cause the structural change of solid.

With an aid of infrared spectroscopy, one can identify the adsorbed species and hence Brønsted acid sites, Lewis acid sites and any other sites. Figure 3 shows the IR difference spectra [(absorbance after adsorption of ammonia) - (absorbance before adsorption of ammonia)] on alumina-

supported-silica monolayer [46] as an example of aluminosilicates possessing both of Brønsted and Lewis acidity [47]. The bands have been attributed based on the vibrations of ammonium salts [48] and ammine complexes [49], quantum chemical calculations [37] and desorption behaviors [50]. The band at 1450 cm^{-1} is ascribed to symmetric deformation vibration of NH_4 species (classified as ν_4 by Nakamoto [48]). The band observed in 1000-1300 cm^{-1} region is ascribed to symmetric deformation vibration of $NH_3 \rightarrow M$ (M = Lewis acidic metal, classified as δ_s by Nakamoto [49]), whereas the wavenumber is sensitive to the kind of M. On Al-containing materials, it is $NH_3 \rightarrow Al$ giving the band around 1220 cm^{-1}, but only a part of them around 1300 cm^{-1} can be observed on aluminosilicates, because the part at >1240 cm^{-1} is hidden by strong absorption ascribed to asymmetric stretching vibration of Si-O-Si [51]. Hydrogen-bonded ammonia, if it exists, should show a band around 1100 cm^{-1} but is also hidden by Si-O-Si on aluminosilicates [50]. Usually on aluminosilicates, the 1450 and 1300 cm^{-1}-bands are the keys for quantification of Brønsted and Lewis acid sites, respectively.

The peak intensities of 1450 and 1300 cm^{-1}-bands are recorded and differentiated by the temperature to draw curves $-\frac{\mathrm{d}A}{\mathrm{d}T}$, where A and T show the absorbance and temperature (K), respectively. The function $-\frac{\mathrm{d}A}{\mathrm{d}T}$ is pseudo-quantitative but not quantitative, as shown by the unit $cm^{-1}\ K^{-1}$ without including mol. It is related with the concentration of ammonia in the gas phase C_g (mol m^{-3}) by the following equation:

$$C_g = \frac{\pi d^2 \beta}{4 \varepsilon F}\left(-\frac{\mathrm{d}A}{\mathrm{d}T}\right) \tag{3}$$

where π, d, β and F are the circular constant (3.1416), diameter of sample disk (mm), ramp rate (K s^{-1}) and flow rate of carrier gas ($m^3\ s^{-1}$), respectively, and they are constant independently of the kinds of adsorbed species on any solids. The remaining parameter ε is the molar extinction coefficient

(cm^{-1} m^2 mol^{-1}) based on Lambert-Beer law:

$$A = \varepsilon c l \tag{4}$$

where c and l are the concentration of discussed species per unit volume (mol m^{-3}) and light path length (m), respectively. The value of ε depends on the vibration mode and nature of adsorbed species, which may also depend on the nature of site, and therefore the value has not been known before the experiment. In a fact, the values observed for the band at 1450 cm^{-1} for Brønsted acid sites on various solid acids were similar (ca. 900 cm^{-1} m^2 mol^{-1}), while those 1000-1300 cm^{-1} for Lewis acid sites were distributed widely (averagely 700 cm^{-1} m^2 mol^{-1} unless it was perturbated by Si-O-Si vibration) [52].

On the other hand, we can assume that the sum of concentrations of ammonia from all the adsorbed species should be equal to C_g measured by MS over the temperature range as follows:

$$C_g = \sum X_i \left(-\frac{\mathrm{d}A_i}{\mathrm{d}T} \right) \tag{5}$$

where X_i is the suitable coefficient for an adsorbed species i showing the IR band with the intensity is A_i. Here X_i is defined as:

$$X_i = \frac{\pi d^2 \beta}{4 \varepsilon_i F} \tag{6}$$

where ε_i is the molar extinction coefficient (cm^{-1} m^2 mol^{-1}) of i.

Because each $-\frac{\mathrm{d}A_i}{\mathrm{d}T}$ have their unique temperature dependency, the set of coefficients X_i

giving the best fitting between C_g measured by MS and $\sum X_i\left(-\frac{\mathrm{d}A_i}{\mathrm{d}T}\right)C_g$ can be obtained by a numerical technique such as minimum squire method as shown in Figure 4. On the solid acid shown in Figure 4 (silica monolayer), the sum of ammonia from Brønsted and Lewis acid sites well related with the major part of total desorption profile recorded by MS [47]. Another example is shown in Figure 2. In this case (SSZ-16, aluminosilicate zeolite with AFX structure), the *l*-peak could not be fitted, indicating that it was ascribed to the hydrogen-bonded species with the IR band hidden by Si-O-Si vibration [35]. By these treatments, one can obtain IRMS-TPD profiles $C_g = \frac{\pi d^2 \beta}{4\varepsilon F}\left(-\frac{\mathrm{d}A}{\mathrm{d}T}\right)$ of each of Brønsted and Lewis acid sites. The value is now quantitatively shown by the unit of vertical axis as mol m^{-3}. Simultaneously, the molar extinction coefficient is estimated.

The amount A_0 (in other words, number of sites, mol kg^{-1}) of each of Brønsted and Lewis acid site is calculated as follows:

$$A_0 = \frac{F}{\beta W}\int C_g \mathrm{d}T \tag{7}$$

where W is the amount of solid employed for the measurement (kg).

Quantitative evaluation of acid strength requires discussion. The TPD process is classified into three cases; [I] kinetic control, [II] equilibrium control, and [III] diffusion control [53]. Niwa et al. found that, in ordinal conditions on various zeolites [54,55] and non-zeolitic solid acids [45,56], the ammonia TPD process was in the class of [II], controlled by equilibrium; it was found from the dependence of peak maximum temperature T_m (K) on the W/F ratio. Masuda et al. found that the activation barrier of adsorption-desorption of ammonia on zeolites are ca. 15 kJ mol^{-1} [57], while the desorption enthalpy is more than 100 kJ mol^{-1}, suggesting that the activation barrier is sufficiently small not to affect the practical influence on the apparent desorption rate.

The control by equilibrium means that T_m depends not only on the experimental conditions

(W, F and β) but also on A_0, a nature of sample. In other words, the re-adsorption of ammonia from the gas phase affects the desorption temperature. On very simple consideration, it disturbs the observation of desorption behavior, giving a disadvantage of the ammonia TPD [40]. However, it should be emphasized that the equilibrium control conditions give parameters describing position of the equilibrium of protonation by Brønsted acid site or coordination to Lewis acid site, which should be the index of acid strength according to the original definition as stated in the previous section.

During the desorption, equilibrium exists between the adsorbed species (NH_3) and a pair of gas molecule and vacant site ( ).

$$(NH_3) \rightarrow NH_3\,(g) + (\quad) \tag{8}$$

The equilibrium constant K can be drawn as

$$K = \frac{a_{(\ )}\, a_{NH_3(g)}}{a_{(NH_3)}} \tag{9}$$

where a_i is the (thermodynamic) activity of species i.

It can be assumed that the activity of any surface species is proportional to the coverage, indicating the following relationship [58].

$$\frac{a_{(\ )}}{a_{(NH_3)}} = \frac{1-\theta}{\theta} \tag{10}$$

where θ is the coverage of acid sites by ammonia.

On the other hand, the activity of gaseous compound is given by the partial pressure relative to the pressure of standard conditions ($P^\circ = 1.013\times10^5$ Pa) [59].

$$a_{\mathrm{NH_3(g)}} = \frac{P}{P^\circ} \tag{11}$$

where P is the partial pressure of ammonia (Pa).

The equation of ideal gas gives the following relation.

$$P = \frac{nRT}{V} = C_g RT \tag{12}$$

where n, V and R are the amount of ammonia (mol), volume of system (m^3) and the gas constant (8.314 J K^{-1} mol^{-1}).

From these relationships, the equilibrium constant can be shown as follows.

$$K = \frac{1-\theta}{\theta}\frac{C_g RT}{P^\circ} \tag{13}$$

It is noteworthy that the above expression is according to Langmuir's theory [58], while a different way of expression by Cvetanović and Amenomiya [53] is also utilized for the analysis of TPD profile. The details are given in Supporting Information.

The equilibrium constant is related with thermodynamic parameters as

$$K = e^{-\frac{\Delta H^\circ}{RT}} e^{\frac{\Delta S^\circ}{R}} \tag{14}$$

where ΔH° is the heat of ammonia adsorption (more exactly, "standard enthalpy change accompanying with desorption", J mol^{-1}), and ΔS° is the standard entropy change accompanying with desorption (J K^{-1} mol^{-1}).

On the other hand, the material balance can be described as

$$FC_g = -\beta A_0 W \frac{\mathrm{d}\theta}{\mathrm{d}T} \tag{15}$$

From the above relationships, eq. (16) is derived.

$$C_g = -\frac{\beta A_0 W}{F}\frac{\mathrm{d}\theta}{\mathrm{d}T} = \frac{\theta}{1-\theta}\frac{P^\circ}{RT}\exp\left(-\frac{\Delta H^\circ}{RT}\right)\exp\left(\frac{\Delta S^\circ}{R}\right) \tag{16}$$

This equation shows C_g as a function of T, namely, a TPD curve. Availability of this equation has been confirmed by experiments on various zeolites [55] and several non-zeolitic solid acid binary oxides [45,56]. Then we found that ΔS° was about 150 J K^{-1} mol^{-1}, almost constant, on various solids [45,55,56], and the validity of value is theoretically supported by thermodynamics [60]. Now we can analyze the value and distribution of ΔH° by curve-fitting between the observed spectrum and C_g simulated based on (16), as shown in Figure 5 [60,61]. Thus determined ΔH°, heat of ammonia adsorption, and its distribution (red line in Figure 6) are the index of acid strength of solid. Numerical solution of the equilibrium-based equation is also given by Masuda et al. [57]

Conversion of ΔH° into Hammett index H_0 [62] is possible by the following equation [56].

$$H_0 = -1.75\times10^{-4}\Delta H^\circ \,/\, \mathrm{J\ mol^{-1}} + 15.9 \tag{17}$$

Figure 6 also shows the thus calculated H_0 on the horizontal axis (upper side).

On the other hand, similar calculation methods for obtaining the distribution of activation barrier of adsorption-desorption assuming the kinetic control conditions have been proposed [63,64]. Unfortunately, they are employed without confirming the kinetic control, and in most cases the experimental conditions are within the range of equilibrium control evidenced as above [54]. It

should be mentioned that the experimental method to perform the kinetic control conditions has been proposed [65]. Further discussion on the numerical analysis methods has been reviewed by Hattori and Ono [13].

As well as the bands of symmetric deformation at 1450 and 1000-1300 cm^{-1}, the asymmetric deformation bands found in 1600-1800 cm^{-1} region are also used for quantification in the cases where the symmetric deformation bands are unclear due to some reasons, e.g., different wavenumber of ammonia on Lewis acid site generated by a hetero metal cation.

Another information can be found in the O-H stretching vibration. A negative band is usually found around 3600 cm^{-1} in the IR difference spectrum on H-form zeolite, ascribed to the consumption of Brønsted acidic OH group by the reaction with ammonia. In some cases, e.g., MOR [66], the acidic OH groups at different crystallographic positions give the IR bands at different wavenumbers. The behavior of recovery of these bands gives us a method for quantification of number and strength of the acidic OH groups at different crystallographic positions. Examples are seen in our papers [31,67-72].

Thus, the ammonia TPD profiles of Brønsted and Lewis acid sites, and furthermore, those of crystallographically non-equivalent OH groups can be obtained. Therefore, the numbers and strength ($\Delta H°$) distributions of Brønsted and Lewis acid sites, and specific OH groups can be obtained by means of the ammonia IRMS-TPD.

We have applied the ammonia IRMS-TPD method to various solid acid catalysts including zeolites with various framework types and compositions. Some interesting findings covering solid acids other than aluminosilicates are shown here.

Figure 7 shows change in the amounts of Brønsted and Lewis acid sites by chemical vapor deposition of silica on γ-alumina. It has been known that a monolayer of silica grew with 0 to 12 Si atoms nm^{-2}, and the monolayer almost completely covers the surface with 12 Si atoms nm^{-2} [73-75]. Further deposition forms doubly accumulated layer. On the other hand, catalytic activities for double bond isomerization of butene, and dealkylation of cumene (2-phenylpropane) and

hexadecylnaphthalene are created by the CVD of silica and show the maximum at 12 Si atoms nm^{-2}. These clearly point out that the monolayer has Brønsted acidity which are the active sites [47]. The quantification of Brønsted and Lewis acid sites brought the clear conclusion on the thin silica layer, investigated as unique aluminosilicate catalyst or catalyst support [47,73-89].

Figure 6 displays the Brønsted acid strength distributions of a typical zeolite (MFI) and the sulfated zirconia. The distribution on the zeolite is narrow as shown by the fact that most of Brønsted acid sites had the ammonia desorption enthalpy in 130-150 kJ mol^{-1}. On the contrary, the non-zeolitic acid catalyst, sulfated zirconia, had a wide distribution of Brønsted acid strength. On the other hand, an acid with H_0 lower (larger negative) than -12 is called superacid [90]. Presence of superacidity or super Brønsted acidity on the sulfated zirconia has been a subject of discussion. Findings consistent with the presence of superacidity have been reported [9,91-95], while those consistent with the lack of superacidity [96-104] have been obtained. Figure 6 tells us that the super Brønsted acid sites with $H_0 < -12$ exist, and the averaged H_0 of Brønsted acid sites is around -11 which is not categorized as the superacid. This solves the controversy [61].

The relationship between the acid strength and catalytic activity per site, or lack of the clear relationship between them have been reported and discussed from various viewpoints, as reviewed [9,11,13,33]. Excellent works have been carried out also on the relationship between the catalytic activity and ammonia desorption enthalpy (adsorption heat) [105]. Here some recent examples are shown.

Based on H/D exchange and other techniques, Louis et al. clarified that the cracking of alkane on a solid Brønsted acid catalyst was initiated by the protonation like a superacid-catalyzed mechanism [106]. Catalytic activity of small alkane cracking in mono-molecular mechanism conditions is related with the ammonia desorption enthalpy of Brønsted acid sites on various zeolites and non-zeolitic solid acid catalysts [107]. High ammonia desorption enthalpy gives low activation enthalpy of the reaction as shown in Figure 8, equivalent to that the stronger the Brønsted acid sites, the higher the activity per site. The linear relationship between the activation enthalpy and ammonia

desorption enthalpy covered FAU, *BEA, MOR and non-zeolitic structures, but the MFI showed exceptional behaviors probably due to the small pore size in the case shown in Figure 8 [108].

The ammonia IRMS-TPD analysis allows us to calculate the kinetic parameter normalized by the number of active sites, which can be assumed to be equivalent to the number of Brønsted acid sites. The activation entropy thus determined shows the loss of freedom of reactant molecule by formation of transition state on the active site. In the small alkane cracking [108], cumene dealkylation and toluene disproportionation [109], compensatory relationship was found between the activation enthalpy and entropy. Contributions of the acid strength, structure of transition state and shape of reaction field can be discussed using the entropy-enthalpy relationship [109-112], as clarified by the advances in host-guest chemistry [113].

3. Principles in Brønsted acid amount and strength of zeolite

Figure 9 shows the plots of Brønsted acid amount against [Al] in H-form zeolites or [Al]-[Na] in HNa-form zeolites. It is noteworthy that the deconvolution of desorption peak based on the desorption temperature (dividing the *l*- and *h*-peaks) was not carried out here, while the Brønsted acid sites were quantified based on the IRMS technique. The number of Brønsted acid site was approximately equal to the number of Al atoms free from Na [114].

It has been believed that excess of Al or distance between two Al atoms shorter than a critical value weakens the acid strength [115]. In a fact, the acid amount less than [Al] is observed by usual procedure of H-form preparation and storage [38], but it is due to the dealumination at high density of acid sites caused by humidity even at the room temperature [116,117]. Careful treatment avoiding the H-form zeolite from exposure to humid atmosphere keeps the stoichiometry between the Brønsted acid site and Al, indicating that a Brønsted acid site is generated by isomorphous substitution of one tetravalent Si atom with a trivalent Al atom [114,118].

Figure 10 shows the plots of averaged ammonia desorption enthalpy of Brønsted acid sites against [Al]-[Na]. The enthalpy is generally dependent on the framework types as MOR > MFI >

*BEA > FAU. The enthalpy is changed by varying [Al] or [Na] within ±8 kJ mol^{-1}, while the difference in enthalpy among zeolites with different framework type is in the order of 10 kJ mol^{-1}. In detail, the enthalpy was slightly decreased with increasing [Al] (not found in Figure 10 directly) [60], but far significant difference in the acid strength (ammonia desorption enthalpy) is caused by the framework structure. More than 50 kJ mol^{-1} of difference in the ammonia desorption enthalpy was observed on various zeolites [34,52].

It should be noteworthy that the above story is not available to a sample with considerable amount of extra-framework multivalent cations. From experiments and quantum chemical calculations, it has been clarified that the ammonia desorption enthalpy of Brønsted acidic OH at O1 position of FAU (Y) zeolite was enhanced by introduction of Ca^{2+}, Ba^{2+}, $LaOH^{2+}$ and $AlOH^{2+}$ into the sodalite cage next to the acid site [70]. Various direct and indirect influences of the extra-framework cations on catalytic activity are observed [119-123], and among them, the strong influence of the extra-framework Al species on the Brønsted acid strength of zeolite has been reported [9,70,124-127]. These effects are exceptional from a view of the effect of framework structure, but the catalytic activity of ultrastable Y (USY) zeolite would be generated by these effects [126]. Because of the importance of USY zeolite in the history of zeolite, the effects of extra-framework species on the Brønsted acid strength should be emphasized.

It is surprising that the acid strength (ammonia desorption enthalpy) is significantly changed by the framework type even at the same composition of zeolite. However, the framework type determines only the way of connection among atoms, i.e., topology, difficult to be related directly with chemical nature such as acid strength. It is speculated that the framework topology generates mechanical forces such as stress, compression and torsion around the ion exchange sites, resulting in unique interatomic distances and angles dependently on the crystallographic position and type of crystal structure. Advances in quantum chemistry is now unveiling the relationships among the structural and chemical features as follows.

Based on cluster models $(HO)_3SiOHAl(OH)_3$, Senchenya et al. showed that the short Al-O

distance and large Si-O-Al angle resulted in the low deprotonation energy, meaning high Brønsted acid strength [128]. We calculated the optimized structures and energies of models of ion exchange sites in their H- and NH_4-forms cut from real zeolite structures. The short Al-O distance brought the high ammonia desorption energy (Figure 11) [129]; here the energy ($\Delta U°$) of ammonia desorption is treated, and it should have the same trend as the enthalpy and practically equivalent value due to the following equation.

$$\Delta U° = \Delta H° - P°\Delta V° \quad (14)$$

where $\Delta V°$ is the increase of volume by desorption of ammonia in the standard conditions, and therefore $P°\Delta V°$ is only about 4 kJ mol^{-1} at 500 K.

In addition, the relationships among geometrical parameters suggest that the short Al-O distance was due to the compression from the both ends of SiOAl unit [129]. The narrow distribution of ammonia desorption enthalpy of Brønsted acid sites in one zeolite is found in most cases as stated in the previous section. This can be explained as that the compression and stress tend to be averaged in one crystallite where all the atoms are connected through strong covalent bonds, leading the similar ammonia adsorption energies for all the Brønsted acid sites within a crystallite. Lower Brønsted acid strength of silicoaluminophosphate (SAPO) than that on the aluminosilicate analogue was explained according to this concept [35]. Based on this concept, the ammonia desorption energy can be predicted from the geometrical parameters in the purely siliceous analogue of the discussed zeolite, and those parameters are found in the database of known [130] or hypothesized [131] zeolite structures. Possibility of selecting candidates of strong Brønsted acid sites from many structures in the database has been reported [132].

On the other hand, Born-Haber cycle like expression of the ammonia desorption is drawn as Figure 12. Among the elementary steps, (A) deprotonation and (C) desolvation of NH_4^+ may be influenced by the nature of solid and site. The former (A) should be important, because it shows the

intrinsic acid strength, whereas the latter (C) is also important because it corresponds to the original definition of acid strength according to Brønsted [1] or Hammett [62]. Multiple factors may be hidden in behavior of an OH group in zeolite as a Brønsted acid. Inconsistent observations are sometimes reported from the characterization of Brønsted acid strength with different techniques. Brändle and Sauer pointed out that trend in the ammonia desorption energy on different zeolites was not related with (A) [133]. It means that the ammonia desorption energy (or enthalpy) is a parameter mainly showing the degree of stabilization of cation (C), namely the ion strength. Here it is noteworthy that (C) may contain special steric effect such as steric hindrance and confinement effect due to the fitting or mismatching of shapes of ammonium cation and cavity, however the above finding (the shorter the Al-O distance, the higher the ammonia desorption energy) indicates that the trend of ammonia desorption energy is independent of the pore size. It can be explained that the compression from the both ends of SiOAl unit makes the anion form (Z^- in Figure 12) stable, because Z^- has Al-O distance always shorter than that in H-Z [129].

4. Conclusion

H-form zeolite consists of only a few kinds of ubiquitous elements, Si, O, Al and H. Dependence of the chemical nature of ion exchange site, e.g., Brønsted acid strength, on the structure and composition of aluminosilicate has been unclear. Nowadays, advances in the measurement techniques, e.g., ammonia IRMS-TPD, and quantum chemical calculations are topics in the studies in this field. The relationships among the composition, structure and acidic property are being clarified. It has been clarified that isomorphous substitution of one Si atom by one Al atom generates one Brønsted acid site. The ammonia desorption energy (enthalpy) is mainly dependent on the framework type, because the compression from the both ends of SiOAl unit stabilizes the anion form. Very small difference in the interatomic distances and angles has an impact; Figure 11 indicates that only 0.1 Å (10 pm) of the difference in Al-O distance results in ca. 20 kJ mol^{-1} of the difference in the ammonia desorption energy. Extra-framework divalent cations including $AlOH^{2+}$

modify the strength of Brønsted acid site being close to the cation.

Acknowledgement: This study was partly supported by JSPS (Japan Society for Promotion of Science) KAKENHI 16H04568 and 16K14093.

1 J. N. Brönsted, Einige Bemerkungen über den Begriff der Säuren und Basen, Recueil des Travaux Chimiques des Pays-Bas. 42 (1923) 718-728.

2 T.M. Lowry, The uniqueness of hydrogen, J. Soc. Chem. Ind. 42 (1923) 43-47.

3 G.N. Lewis, Valence and The Structure of Atoms and Molecules, Chemical Catalogue Company, New York, 1923.

4 S.D. Burd, Jr., J. Mazuik, Selectoforming gasoline and LPG, Hydrocarbon Process. 51 (1972) 97-102.

5 V.J. Frilette, W.O. Haag, R.M. Lago, Catalysis by crystalline aluminosilicates: Characterization of intermediate pore-size zeolites by the "Constraint Index", J. Catal. 67 (1982) 218-222.

6 L.A. Pine, P.J. Maher, W.A. Wachter, Prediction of cracking catalyst behavior by a zeolite unit cell size model, J. Catal. 85 (1984) 466-476.

7 J. Scherzer, A.J. Gruia, Hydrocracking Science and Technology, Marcel Dekker, New York, 1996.

8 J. Houžvičla, V. Ponec, Skeletal Isomerization of n-Butene, Catal. Rev.-Sci. Eng. 39 (1997) 319-344.

9 A. Corma, Inorganic Solid Acids and Their Use in Acid-Catalyzed Hydrocarbon Reactions, Chem. Rev. 95 (1995) 559-614.

10 I.E. Maxwell, W.H.J. Stork, Hydrocarbon processing with zeolites, Stud. Surf. Sci. Catal. 137 (2001) 747-819.

11 K. Tanabe, Solid Acids and Bases: Their Catalytic Properties, Kodansha, Tokyo, 1971.

12 K. Tanabe, M. Misono, H. Hattori, Y. Ono, New Solid Acids and Bases: Their Catalytic Properties, Kodansha, Tokyo, 1989.

13 H. Hattori, Y. Ono, Solid Acid Catalysis: From Fundamentals to Applications, CRC Press, Boca

Raton, 2015.

14 A. Corma, B.W. Wojciechowski, The Catalytic Cracking of Cumene, Catal. Rev. Sci. Eng. 24 (1982) 1-65.

15 J.S. Beck, D.H. Olson, S.B. McCullen, Selective Toluene Disproportionation Process (STDP) with ex-situ Selectivated Zeolite Catalyst, U. S. Patent 5367099, 1994.

16 T.-C. Tsai, S.-B. Liu, I. Wang, Disproportionation and Transalkylation of Alkylbenzenes over Zeolite Catalysts, Appl. Catal., A: Gen. 181 (1999) 355-398.

17 F. Zhao, Y. Zhang, S. D. Geng, L. F. Chen, W. Wang, Structure, Acid Properties and Catalysis Performance of MCM-22 Family Zeolites on the Alkylation of Benzene with Propylene, Adv. Mater. Res. 549 (2012) 283-286.

18 S. Al-Khattaf, S.A. Ali, A.M. Aitani, N. Žilková, D. Kubička, J. Čejka, Recent Advances in Reactions of Alkylbenzenes Over Novel Zeolites: The Effects of Zeolite Structure and Morphology, Catal. Rev. Sci. Eng. 56 (2014) 333-402.

19 H. Ishida, Liquid-phase hydration process of cyclohexene with zeolites, Catal. Surveys Jpn. 1 (1997) 241-246.

20 Y. Ashina, T. Fujita, M. Fukatsu, K. Niwa, J. Yagi, Manufacture of Dimethylamine Using Zeolite Catalyst, Stud. Surf. Sci. Catal. 28 (1986) 779-786.

21 H. Tsuneki, Development of Diethanolamine Selective Production Process Using Shape-Selective Zeolite Catalyst, Catal. Surveys Asia 14 (2010) 116-123.

22 N. Katada, S. Kuroda, M. Niwa, High Catalytic Activity for Synthesis of Aniline from Phenol and Ammonia Found over Gallium-containing MFI, Appl. Catal. A: Gen. 180 (1999) L1-L3.

23 S. Shimizu, N. Abe, A. Iguchi, H. Sato, Synthesis of pyridine bases: general methods and recent advances in gas phase synthesis over ZSM-5 zeolite, Catal. Surveys Jpn. 2 (1998) 71-76.

24 H. Ichihashi, M. Ishida, A. Shiga, M. Kitamura, T. Suzuki, K. Suenobu, K. Sugita, The catalysis of vapor-phase Beckmann rearrangement for the production of ε-caprolactam, Catal. Surveys Asia 7 (2003) 261-270.

25 J.C. Védrine, Acid-Base Characterization of Heterogeneous Catalysts: an Up-to-Date Overview, Res. Chem. Interm. 41 (2015) 9387-9423.

26 R. Yoshimoto, K. Hara, K. Okumura, N. Katada, Miki Niwa, Analysis of Toluene Adsorption on Na-form Zeolite Using Temperature-Programmed Desorption Method, J. Phys. Chem. 111 (2007) 1474-1479.

27 K. Okumura, K. Kato, T. Sanada, M. Niwa, In-situ QXAFS Studies on the Dynamic Coalescence and Dispersion Processes of Pd in the USY Zeolite, J. Phys. Chem. C 111 (2007) 14426-14432.

28 K. Okumura, T. Tomiyama, S. Okuda, H. Yoshida, M. Niwa, Origin of the Excellent Catalytic Activity of Pd Loaded on Ultra-Stable Y Zeolites in Suzuki-Miyaura Reactions, J. Catal. 273 (2019) 156-166.

29 A. Oda, H. Torigoe, A. Itadani, T. Ohkubo, T. Yumura, H. Kobayashi, Y. Kuroda, Unprecedented Reversible Redox Process in the ZnMFI-H_2 System Involving Formation of Stable Atomic Zn^0, Angew. Chem. Intl. Ed. 51, (2012) 7719-7723.

30 B. Louis, S. Walspurger, J. Sommer, Quantitative determination of Bronsted acid sites on zeolites: a new approach towards the chemical composition of zeolites, Catal. Lett. 93 (2004) 81-84.

31 M. Niwa, K. Suzuki, N. Katada, T. Kanougi, T. Atoguchi, Ammonia IRMS-TPD study on the distribution of acid sites in mordenite, J. Phys. Chem. B 109 (2005) 18749-18757.

32 C.A. Emeis, Determination of Integrated Molar Extinction Coefficients for Infrared Absorption Bands of Pyridine Adsorbed on Solid Acid Catalysts, J. Catal. 141 (1993) 347-354.

33 G. Busca, Heterogeneous Catalytic Materials, 1st Edition: Solid State Chemistry, Surface Chemistry and Catalytic Behaviour, Elsevier, Amsterdam, 2014.

34 M. Niwa, N. Katada, New Method for the Temperature-Programmed Desorption (TPD) of Ammonia Experiment for Characterization of Zeolite Acidity: A Review, Chem. Rec. 13 (2013) 432-435.

35 N. Katada, K. Nouno, J.K. Lee, J. Shin, S.B. Hong, M. Niwa, Acidic Properties of Cage-Based, Small-Pore Zeolites with Different Framework Topologies and Their Silicoaluminophosphate

Analogues, J. Phys. Chem. C 115 (2011) 22505-22513.

36 W.L. Earl, P.O. Fritz, A.A.V. Gibson, J.H. Lunsford, A solid-state NMR study of acid sites in zeolite Y using ammonia and trimethylamine as probe molecules, J. Phys. Chem. 91 (1987) 2091-2095.

37 A. Zecchina, L. Marchese, S. Bordiga, C. Pazè, E. Gianotti, Vibrational Spectroscopy of NH_4^+ Ions in Zeolitic Materials: An IR Study, J. Phys. Chem. B 101 (1997) 10128-10135.

38 H. Igi, N. Katada, M. Niwa, Principle for Generation of Acidity in Y Zeolite Found by Ammonia Temperature-Programmed Desorption: Stoichiometric Generation of Acid Sites with a Constant Strength by Isolated Framework Al Atoms, in: M.M.J. Treacy, B.K. Marcus, M.E. Bisher, J.B. Higgins (Eds.), Proceedings of the 12th International Zeolite Conference, Materials Research Society, Warrendale, 1999, pp. 2643-2650.

39 J. Valyon, Gy. Onyestyák, L.V.C. Rees, A Frequency-Response Study of the Diffusion and Sorption Dynamics of Ammonia in Zeolites, Langmuir 16 (2001) 1331-1336.

40 R.J. Gorte, What do we know about the acidity of solid acids? Catal. Lett. 62 (1999) 1-13.

41 G. Bagnasco, Improving the Selectivity of NH_3TPD Measurements, J. Catal. 159 (1996) 249-252.

42 G.L. Woolery, G.H. Kuehl, H.C. Timken., A.W. Chester, J.C. Vartuli, On the nature of framework Brønsted and Lewis acid sites in ZSM-5, Zeolites 19 (1997) 288-296.

43 A. Kohara, N. Katada, M. Niwa, Very Strong Acid Site in HZSM-5 Formed during the Template Removal Step; Its Control, Structure and Catalytic Activity, Stud. Surf. Sci. Catal. 135 (2001) 341.

44 M. Niwa, N. Morishita, H. Tamagawa, N. Katada, HZSM-5 Treated with Ammonia and Water Vapor; Characterization and Cracking Activity, Catal. Today 198 (2012) 12-18.

45 N. Naito, N. Katada, M. Niwa, Tungsten Oxide Monolayer Loaded on Zirconia: Determination of Acidity Generated on the Monolayer, J. Phys. Chem. B 103 (1999) 7206-7213.

46 M. Niwa, T. Hibino, H. Murata, N. Katada, Y. Murakami, A Silica Monolayer on Alumina and Evidence of Lack of Acidity of Silanol Attached to Alumina, J. Chem. Soc. Chem. Commun. (1989) 289-290.

47 N. Katada, Y. Kawaguchi, K. Takeda, T. Matsuoka, N. Uozumi, K. Kanai, S. Fujiwara, K. Kinugasa, K. Nakamura, S. Suganuma, M. Nanjo, Dealkylation of Alkyl Polycyclic Aromatic Hydrocarbon over Silica Monolayer Solid Acid Catalyst, Appl. Catal. A: Gen. 530 (2017) 93-101.

48 K. Nakamoto, Infrared and Raman Spectra of Inorganic and Coordination Compounds, 6th Edition, Part A, John Wiley & Sons, Hoboken, 2009.

49 K. Nakamoto, Infrared and Raman Spectra of Inorganic and Coordination Compounds, 6th Edition, Part B, John Wiley & Sons, Hoboken, 2009.

50 S. Suganuma, Y. Murakami, J. Ohyama, T. Torikai, K. Okumura, N. Katada, Assignments of Bending Vibrations of Ammonia Adsorbed on Surfaces of Metal Oxides, Catal. Lett. 145 (2015) 1904-1912.

51 B.C. Smith, Infrared Spectral Interpretation: A Systematic Approach, CRC Press, Boca Raton, 1998.

52 M. Niwa, N. Katada, K. Okumura, Characterization and Design of Zeolite Catalysts: Solid Acidity, Shape Selectivity and Loading Properties, Springer, Berlin, 2010.

53 R.J. Cvetanović, Y. Amenomiya, Application of a Temperature-Programmed Desorption Technique to Catalyst Studies, Adv. Catal. 17 (1967) 103-149.

54 M. Niwa, M. Iwamoto, K. Segawa, Temperature-Programmed Desorption of Ammonia on Zeolites. Influence of the Experimental Conditions on the Acidity Measurement, Bull. Chem. Soc. Jpn., 59 (1986) 3735-3739.

55 M. Niwa, N. Katada, M. Sawa, Y. Murakami, Temperature-Programmed Desorption of Ammonia with Readsorption Based on the Derived Theoretical Equation, J. Phys. Chem. 99 (1995) 8812-8816.

56 N. Katada, J. Endo, K. Notsu, N. Yasunobu, N. Naito, M. Niwa, Superacidity and Catalytic Activity of Sulfated Zirconia, J. Phys. Chem. B 104 (2000) 10321-10328.

57 T. Masuda, Y. Fujikata, S.R. Mukai, K. Hashimoto, A method of calculating adsorption enthalpy distribution using ammonia temperature-programmed desorption spectrum under adsorption equilibrium conditions, Appl. Catal. A: Gen. 165 (1997) 57-72.

58 I. Langmuir, Surface Chemistry, Chem. Rev. 13 (1933) 147-191.

59 C.R. Metz, Theory and Problems of Physical Chemistry, McGraw-Hill, New York, 1976 p. 82.

60 N. Katada, H. Igi, J.-H. Kim, M. Niwa, Determination of the Acidic Properties of Zeolite by Theoretical Analysis of Temperature-Programmed Desorption of Ammonia Based on Adsorption Equilibrium, J. Phys. Chem. B 101 (1997) 5969-5977.

61 N. Katada, T. Tsubaki, M. Niwa, Measurements of Number and Strength Distribution of Brønsted and Lewis Acid Sites on Sulfated Zirconia by Ammonia IRMS-TPD Method, Appl. Catal. A: Gen. 340 (2008) 76-86.

62 L.P. Hammett, A.J. Deyrup, A Series of Simple Basic Indicators. I. The Acidity Functions of Mixtures of Sulfuric and Perchloric Acids with Water, J. Am. Chem. Soc. 54 (1932) 2721-2739.

63 H.G. Karge, V. Dondur, J. Weitkamp, Investigation of the distribution of acidity strength in zeolites by temperature-programmed desorption of probe molecules. 2. Dealuminated Y-type zeolites, J. Phys. Chem. 95 (1991) 283-288.

64 C. Costa, J.M. Lopes, F. Lemos, F. Ramôa Ribeiro, Activity-acidity relationship in zeolite Y: Part 2. Determination of the acid strength distribution by temperature programmed desorption of ammonia, Appl. Catal. A: Gen. 144 (1999) 221-231.

65 T. Masuda, Y. Fujikata, H. Ikeda, S. Matsushita, K. Hashimoto, A method for calculating the activation energy distribution for desorption of ammonia using a TPD spectrum obtained under desorption control conditions, Appl. Catal. A: Gen. 162 (1997) 29-40.

66 A. Alberti, Location of Brønsted sites in mordenite, Zeolite 19 (1997) 411-415.

67 M. Niwa, K. Suzuki, K. Isamoto, N. Katada, Identification and Measurements of Strong Brønsted Acid Site in Ultrastable Y (USY) Zeolite, J. Phys. Chem. B 110 (2006) 264-269.

68 K. Suzuki, N. Katada, M. Niwa, Detection and Quantitative Measurements of Four Kinds of OH in HY Zeolite, J. Phys. Chem. C 111 (2007) 894-900.

69 K. Suzuki, G. Sastre, N. Katada, M. Niwa, Ammonia IRMS-TPD Measurements and DFT Calculation on Acidic Hydroxyl Groups in CHA-type Zeolite, Phys. Chem. Chem. Phys. 9 (2007)

5980-5987.

70 K. Suzuki, T. Noda, G. Sastre, N. Katada, M. Niwa, Periodic Density Functional Calculation on Brønsted Acidity of Modified Y-type Zeolite, J. Phys. Chem. C 113 (2009) 5672-5680.

71 K. Suzuki, N. Katada, M. Niwa, Measurements of Acidity of H-SSZ-35 by a Combined Method of IRMS-TPD Experiment and DFT Calculation, Catal. Lett. 140 (2010) 134-139.

72 N. Katada, H. Tamagawa, M. Niwa, Number and Brønsted Acid Strength of Bridging OH Groups with Different Stretching Frequencies in Zeolite β Analyzed by Ammonia IRMS-TPD Measurement and DFT Calculations, Catal. Today. 226 (2014) 37-46.

73 M. Niwa, N. Katada, Y. Murakami, Thin Silica Layer on Alumina: Evidence of the Acidity in the Monolayer, J. Phys. Chem. 94 (1990) 6441-6445.

74 N. Katada, T. Toyama, M. Niwa, Mechanism of Growth of Silica Monolayer and Generation of Acidity by Chemical Vapor Deposition of Tetramethoxysilane on Alumina, J. Phys. Chem. 98 (1994) 7647-7652.

75 N. Katada, M. Niwa, The Re-birth of Molecular Imprinting on Silica, S. Piletsky, A. Turner, I. Nicholls (eds.) Molecular Imprinting of Polymers, Landes Bioscience / Eurekah. Com., Georgetown, 2005, pp. 26-40.

76 T. Jin, T. Okuhara, J.M. White, Ultra-high vacuum preparation and characterization of ultra-thin layers of SiO_2 on ZrO_2 and TiO_2 by chemical vapour deposition of $Si(OEt)_4$, J. Chem. Soc. Chem. Commun. (1987) 1248-1249.

77 B.-Q. Xu, T. Yamaguchi, K. Tanabe, Dehydrogenation of Alkylamines on Acid-Base Hybrid Catalyst, Chem. Lett. 18 (1989) 149-152.

78 S. Sato, M. Toita, Y.-Q. Yu, T. Sodesawa, F. Nozaki, Catalytic Properties of Silica-Alumina Prepared by Chemical Vapor Deposition, Chem. Lett. 16 (1987) 1535-1536.

79 H. Fukui, T. Ogawa, M. Nakano, M. Yamaguchi, Y. Kanda, Formation of Polymethylsiloxane Network on Metal Oxides by Chemical Vapor Deposition of 1,3,5,7-Tetramethylcyclotetrasiloxane, H. Ishida (ed.) Controlled Interphases in Composite Materials, Elsevier, Amsterdam, 1990. pp. 469-

478.

80 B. Beguin, E. Garbowski, M. Primet, Stabilization of alumina toward thermal sintering by silicon addition, J. Catal. 127 (1991) 595-604.

81 P. Sarrazin, S. Kasztelan, N. Zanier-Szydlowski, J.P. Bonnelle, J. Grimblot, Interaction of oxomolybdenum species with γ-alumina and γ-alumina modified by silicon. 1. The silica γ-alumina system, J. Phys. Chem. 97 (1993) 5947-5953.

82 T. Horiuchi, T. Sugiyama, T. Mori, Factors for maintenance of a high surface area of silica-coated α-alumina after heating >1573 K, J. Mater. Chem. 3 (1993) 861-865.

83 T.C. Sheng, I.D. Gay, Measurement of Surface Acidity by ^{31}P NMR of Adsorbed Trimethylphosphine: Application to Vapor Deposited SiO_2 on Al_2O_3 Monolayer Catalysts, J. Catal. 145 (1994) 10-15.

84 N. Okazaki, T. Kohno, R. Inoue, Y. Imizu, A. Tada, Enhanced Catalytic Activity of Silica-Deposited Alumina for Selective Reduction of Nitrogen Monoxide by Ethene in Oxidizing Atmosphere, Chem. Lett. 22 (1993) 1195-1198.

85 N. Katada, H. Ishiguro, K. Muto, M. Niwa, Heat-Resisting Acid Catalyst: Thermal Stability and Acidity of Thin Silica Layer on Alumina Calcined at 1493 K, Chem. Vap. Deposition 1 (1995) 54-60.

86 S. Yamakita, N. Katada, M, Niwa, Shape-Selective Adsorption of Substituted Benzaldehyde Isomers by a Molecular Sieving Silica Overlayer Prepared by the Chemical Vapor Deposition Method Using Organic Template on Tin Oxide, Bull. Chem. Soc. Jpn. 78 (2005) 1425-1430.

87 M. Sekiyama, N. Katada, M. Niwa, Molecular Shape-Selective Detection by Tin Oxide Film Sensor Modified with Chemical Vapor Deposition of Molecular-Sieving Silica Overlayer Using Organic Template, Sens. Actuators B: Chem. 124 (2007) 398-406.

88 A.R. Mouat, C. George, T. Kobayashi, M. Pruski, R.P. van Duyne, T.J. Marks, P.C. Stair Highly Dispersed SiO_x/Al_2O_3 Catalysts Illuminate the Reactivity of Isolated Silanol Sites, Angew. Chem. Int. Ed. 54 (2015) 13346-13351.

89 M.A. Ardagh, Z. Bo, S.L. Nauert, J.M. Notestein, Depositing SiO_2 on Al_2O_3: a Route to Tunable Brønsted Acid Catalysts, ACS Catal. 6 (2016) 6156-6164.

90 J.B. Conant, N.F. Hall, A Study of Superacid Solutions. II. A Chemical Investigation of the Hydrogen-ion Activity of Acetic Acid Solutions, J. Am. Chem. Soc. 49 (1927) 3062-3070.

91 K. Arata, Solid Superacids, Adv. Catal. 37 (1990) 165-211.

92 F.R. Chen, G. Coudurier, J.F. Joly, J.C. Vedrine, Superacid and Catalytic Properties of Sulfated Zirconia, J. Catal. 143 (1993) 616-626.

93 T. Riemer, D. Spielbauer, M. Hunger, G.A.H. Mekhemer, H. Knözinger, Superacid properties of sulfated zirconia as measured by Raman and ^{1}H MAS NMR spectroscopy, J. Chem. Soc. Chem. Commun. (1994) 1181-1182.

94 T. Riemer, H. Knözinger, ^{31}P Solid State NMR and ESR Investigation of Trimethylphosphane Adsorption on Zirconia and Sulfated Zirconia, J. Phys. Chem. 100 (1996) 6739-6742.

95 D. Fraenkel, Acid Strength of Sulfated Zirconia Inferred from Catalytic Isobutane Conversion, Chem. Lett. (1999) 917-918.

96 B. Umansky, J. Engelhardt, W.K. Hall, On the strength of solid acids, J. Catal. 127 (1991) 128-140.

97 F. Babou, B. Bigot, P. Sautet, The superacidity of sulfated zirconia: an ab-initio quantum mechanical study, J. Phys. Chem. 97 (1993) 11501-11509.

98 L.M. Kustov, V.B. Kazansky, F. Figueras, D. Tichit, Investigation of the Acidic Properties of ZrO_2 Modified by SO_4^{2-} Anions, J. Catal. 150 (1994) 143-149.

99 V. Adeeva, J.W. Dehaan, J. Janchen, G.D. Lei, R.A. Vansanten, Acid Sites in Sulfated and Metal-Promoted Zirconium Dioxide Catalysts, J. Catal. 151 (1995) 364-372.

100 V. Adeeva, G.D. Lei, W.M.H. Sachtler, Competitive mechanisms of n-butane isomerization on sulfated zirconia catalysts, Catal. Lett. 33 (1995) 135-143.

101 D. Fărcaşiu, J.Q. Li, A. Kogelbauer, The mechanism of conversion of hydrocarbons on sulfated metal oxides. Part IV. Kinetics of the reaction of methylcyclopentane on sulfated zirconia, J. Mol.

Catal. A: Chem. 124 (1997) 67-78.

102 R.S. Drago, N. Kob, Acidity and Reactivity of Sulfated Zirconia and Metal-Doped Sulfated Zirconia, J. Phys. Chem. B 101 (1997) 3360-3364.

103 V. Adeeva, H.-Y. Liu, B.-Q. Xu, W.M.H. Sachtler, Alkane isomerization over sulfated zirconia and other solid acids, Top. Catal. 6 (1998) 61-76.

104 F. Haase, J. Sauer, The Surface Structure of Sulfated Zirconia: Periodic ab Initio Study of Sulfuric Acid Adsorbed on ZrO_2(101) and ZrO_2(001), J. Am. Chem. Soc. 120 (1998) 13503-13512.

105 A. Gervasini, G. Bellussi, J. Fenyvesi, A. Auroux, Microcalorimetric and catalytic studies of the acidic character of modified metal oxide surfaces. 1. Doping ions on alumina, magnesia, and silica, J. Phys. Chem. 99 (1995) 5117-5125.

106 B. Louis, M.M. Pereira, F.M. Santos, P.M. Esteves, J. Sommer, Alkane Activation over Acidic Zeolites: The First Step, Chem. Eur. J. 16 (2010) 573-576.

107 N. Katada, K. Suzuki, T. Noda, W. Miyatani, F. Taniguchi, M. Niwa, Correlation of the Cracking Activity with Solid Acidity and Adsorption Property on Zeolites, Appl. Catal. A: Gen. 373 (2010) 208-213.

108 N. Katada, S. Sota, N. Morishita, K. Okumura, M. Niwa, Relationship between Activation Energy and Pre-exponential Factor Normalized by Number of Brønsted Acid Sites in Cracking of Short Chain Alkanes on Zeolites, Catal. Sci. Technol. 5 (2015) 1864-1869.

109 N. Katada, K. Nakamura, S. Suganuma, E. Tsuji, Relationship among Structure, Brønsted Acid Strength and Activation Energy in Acid-Catalyzed Reaction on Zeolites, The 7th International FEZA Conference, O38 (2017).

110 F. Eder, J.A. Lercher, On the role of the pore size and tortuosity for sorption of alkanes in molecular sieves. J. Phys. Chem. B 101 (1997) 1273-1278.

111 T. Bucko, J. Hafner, Entropy effects in hydrocarbon conversion reactions: free-energy integrations and transition-path sampling, J. Phys. Condens. Matter 22 (2010) 384201.

112 R. Gounder, E. Iglesia, The Roles of Entropy and Enthalpy in Stabilizing Ion-pairs at Transition

States in Zeolites Acid Catalysts, Acc. Chem. Res. 45 (2012) 229-238.

113 Y. Inoue, Y. Liu, L.H. Tong, B.J. Shen, D.S. Jin, Calorimetric titration of inclusion complexation with modified β-cyclodextrins. Enthalpy-entropy compensation in host-guest complexation: from ionophore to cyclodextrin and cyclophane, J. Am. Chem. Soc. 115 (1993) 10637-10644.

114 N. Katada, Y. Kageyama, M. Niwa, Acidic Property of Y- and Mordenite-type Zeolites with High Aluminum Concentration under Dry Conditions, J. Phys. Chem. B 104 (2000) 7561-7564.

115 D. Barthomeuf, Topology and maximum content of isolated species (Al, Ga, Fe, B, Si, ...) in a zeolitic framework. An approach to acid catalysis, J. Phys. Chem. 97 (1993) 10092-10096.

116 N. Katada, T. Kanai, M. Niwa, Dealumination of Proton Form Mordenite with High Aluminum Content in Atmosphere, Micropor. Mesopor. Mater. 75 (2004) 61-67.

117 N. Katada, T. Takeguchi, T. Suzuki, T. Fukushima, K. Inagaki, S. Tokunaga, H. Shimada, K. Sato, Y. Oumi, T. Sano, K. Segawa, K. Nakai, H. Shoji, P. Wu, T. Tatsumi, T. Komatsu, T. Masuda, K. Domen, E. Yoda, J.N. Kondo, T. Okuhara, Y. Kageyama, M. Niwa, M. Ogura, M. Matsukata, E. Kikuchi, N. Okazaki, M. Takahashi, A. Tada, S. Tawada, Y. Kubota, Y. Sugi, Y. Higashio, M. Kamada, Y. Kioka, K. Yamamoto, T. Shouji, Y. Arima, Y. Okamoto, H. Matsumoto, Standardization of Catalyst Preparation Using Reference Catalyst. Ion Exchange of Mordenite Type Zeolite 1: Remarkable Dealumination Accompanying Ion Exchange, Appl. Catal. A: Gen. 283 (2005) 63-74.

118 N. Katada, T. Takeguchi, T. Suzuki, T. Fukushima, K. Inagaki, S. Tokunaga, H. Shimada, K. Sato, Y. Oumi, T. Sano, K. Segawa, K. Nakai, H. Shoji, P. Wu, T. Tatsumi, T. Komatsu, T. Masuda, K. Domen, E. Yoda, J.N. Kondo, T. Okuhara, T. Kanai, M. Niwa, M. Ogura, M. Matsukata, E. Kikuchi, N. Okazaki, M. Takahashi, A. Tada, S. Tawada, Y. Kubota, Y. Sugi, Y. Higashio, M. Kamada, Y. Kioka, K. Yamamoto, T. Shouji, S. Satokawa, Y. Arima, Y. Okamoto, H. Matsumoto, Standardization of Catalyst Preparation Using Reference Catalyst. Ion Exchange of Mordenite Type Zeolite 2: Origin of Dealumination and Recommended Standard Conditions, Appl. Catal. A: Gen. 283 (2005) 75-84.

119 S.J. DeCanio, J.R. Sohn, P.O. Fritz, J.H. Lunsford, Acid catalysis by dealuminated zeolite-Y: I.

Methanol dehydration and cumene dealkylation, J. Catal. 101 (1986) 132-141.

120 R. Carvajal, P.-J. Chu, J.H. Lunsford, The role of polyvalent cations in developing strong acidity: A study of lanthanum-exchanged zeolites, J. Catal.125 (1990) 123-131.

121 A.I. Biaglow, D.J. Parrillo, G.T. Kokotailo, R.J. Gorte, A Study of Dealuminated Faujasites, J. Catal. 148 (1994) 213-223.

122 U. Lohse, E. Löffler, M. Hunger, J. Stöckner, V. Patzelová, Hydroxyl groups of the non-framework aluminium species in dealuminated Y zeolites, Zeolites 7 (1987) 11-13.

123 B. Xu, S. Bordiga, R. Prins, J.A. van Bokhoven, Effect of framework Si/Al ratio and extra-framework aluminum on the catalytic activity of Y zeolite, Appl. Catal. A: Gen. 333 (2007) 245-253.

124 G. Garralón, A. Corma, V. Formés, Evidence for the presence of superacid nonframework hydroxyl groups in dealuminated HY zeolites, Zeolites 9 (1989) 84-86.

125 D.C. Koningsberger, J.T. Miller, The Development of Strong Acidity by Non-Framework Aluminum in H-USY Determined by Al XAFS Spectroscopy, Stud. Surf. Sci. Catal. 101 (1996) 841-850.

126 N. Katada, Y. Kageyama, K. Takahara, T. Kanai, H.A. Begum, M. Niwa, Acidic property of modified ultra stable Y zeolite: increase in catalytic activity for alkane cracking by treatment with ethylenediaminetetraacetic acid salt, J. Mol. Catal. A: Chem. 211 (2004) 119-130.

127 N. Katada, S. Nakata, S. Kato, K. Kanehashi, K. Saito, M. Niwa, Detection of Active Sites for Paraffin Cracking on USY Zeolite by ^{27}Al MQMAS NMR Operated at High Magnetic Field 16 T, J. Mol. Catal. A: Chem. 236 (2005) 239-245.

128 I.N. Senchenya, V.B. Kazanskii, S. Beran, Quantum chemical study of the effect of the structural characteristics of zeolites on the properties of their bridging hydroxyl groups. Part 2, J. Phys. Chem. 90 (1986) 4857-4859.

129 N. Katada, K. Suzuki, T. Noda, G. Sastre, M. Niwa, Correlation between Brønsted Acid Strength and Local Structure in Zeolites, J. Phys. Chem. C 113 (2009) 19208-19217.

130 International Zeolite Association, Database of Zeolite Structures. http://www.iza-

structure.org/databases/, 2017 (accessed 23.07.17).

131 M.D. Foster, M.M.J. Treacy, Atlas of Prospective Zeolite Structures. http://www.hypotheticalzeolites.net/NEWDATABASE/index.html, 2017 (accessed 23.07.17).

132 T. Matsuoka, L. Baumes, N. Katada, A. Chatterjee, G. Sastre, Selecting Strong Brønsted Acid Zeolites through Screening from a Database of Hypothetical Frameworks, Phys. Chem. Chem. Phys. 19 (2017) 14702-14707.

133 M. Brändle, J. Sauer, Acidity Differences between Inorganic Solids Induced by Their Framework Structure. A Combined Quantum Mechanics/Molecular Mechanics ab Initio Study on Zeolites, J. Am. Chem. Soc. 120 (1998) 1556-1570.

Table 1 Representing methods proposed for measurements of acidic property of solid

		Acid amount	Equilibrium of protonation / coordination	Type	Note
[i]	Indicator	◎	◎	X	Generally difficult for micropores
	Ammonia TPD	◎	◎	X	
	Ammonia calorimetry	◎	◎	X	
	Ar TPD	◎	X*	X	Adsorbed also on base site
	Propyl amine TPD	△	△	△	
	H_2O/D_2O exchange	Brønsted only	Brønsted only	◎	
[ii]	IR of pyridine	X**	X	◎	Not available to <8-ring
	IR of OH	X	Relative value	◎	
	^1H NMR	◎	Relative value	◎	
	IR of CO	X	X*	◎	
	IR of nitrile	X	X*	◎	
[i]+[ii]	Ammonia IRMS-TPD	◎	◎	◎	

◎: can be obtained, △: partly, X: no. *: Strength of physical adsorption can be evaluated. **: Assumption of molar extinction coefficient can give a way of quantification, as shown by Emeis [32].

Figure captions

Figure 1 Schematic drawing of hydrocarbon flow in typical petroleum refinery. Thick rectangles show the processes where aluminosilicates are used as solid acid catalysts.

Figure 2 An example of ammonia IRMS-TPD profile of H-AFX zeolite.

Figure 3 IR difference spectra on silica monolayer supported by alumina. Only the spectra extracted in 10 K interval are displayed, while the measurements were carried out at every 1 K.

Figure 4 Ammonia IRMS-TPD profiles of Brønsted and Lewis acid sites.

Figure 5 Ammonia TPD profile of Brønsted acid sites observed on sulfated zirconia (blue), profiles simulated on different ammonia desorption enthalpies (black lines) and sum of them (red) based on distribution of enthalpy giving best fitted curves.

Figure 6 Distribution of ammonia desorption enthalpy of Brønsted acid sites on sulfated zirconia (red) and H-MFI zeolite (blue). The former was calculated from Figure 5.

Figure 7 Amounts of Brønsted and Lewis acid sites as functions of amount of silica chemically deposited on alumina.

Figure 8 Plots of activation enthalpy of reactions of propane (black), 2-methylpropane (red), butane (brown), 2-methylbutane (green), pentane (grey), hexane (blue) and octane (purple) over FAU (○),

*BEA (▽), MFI (◆), MOR (△) zeolites, amorphous silica-alumina (＋) and sulfated zirconia (×) against enthalpy of ammonia desorption.

Figure 9　Plots of amount of Brønsted acid sites quantified by ammonia IRMS-TPD method against $[Al_F]$-[Na] on various H- and HNa-form zeolites.

Figure 10　Plots of averaged enthalpy of ammonia desorption (ΔH°) of Brønsted acid sites against $[Al_F]$-[Na] on various H- and HNa-form zeolites.　The results not measured by the ammonia IRMS-TPD method but measured by combinations of other techniques are included.

Figure 11　Plots of ammonia desorption energy against Al-O distance calculated on density functional theory on ion exchange sites located at some different crystallographic positions in various zeolite structures.

Figure 12　Energy diagram for ammonia adsorption-desorption divided into assumed elementary steps.　Z shows the ion exchange site.

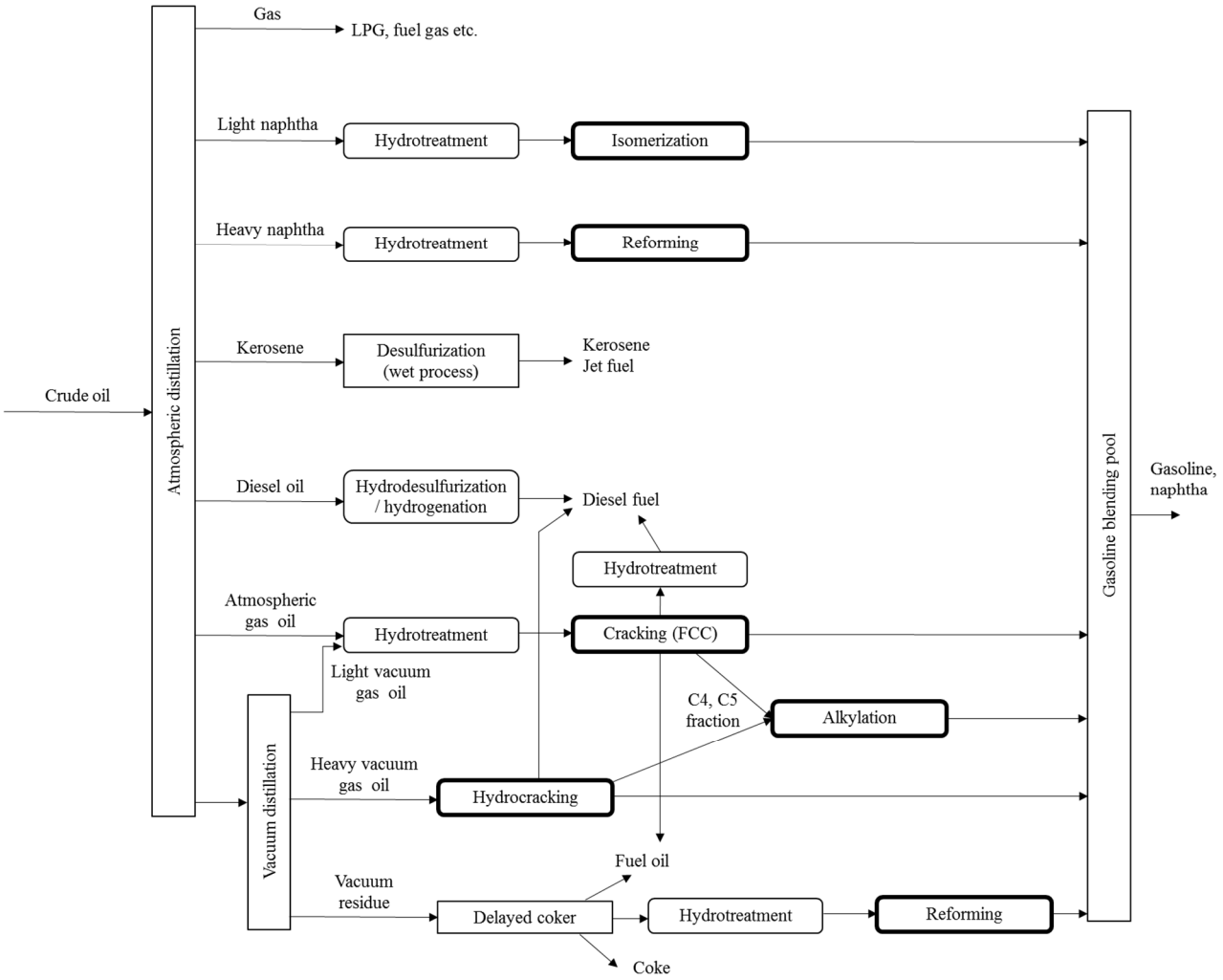
Gas
LPG, fuel gas etc.
Light naphtha
Hydrotreatment
Isomerization
Heavy naphtha
Hydrotreatment
Reforming
Kerosene
Desulfurization
(wet process)
Kerosene
Jet fuel
Crude oil
Atmospheric distillation
Diesel oil
Hydrodesulfurization
/ hydrogenation
Diesel fuel
Hydrotreatment
Atmospheric
gas oil
Hydrotreatment
Cracking (FCC)
Light vacuum
gas oil
C4, C5
fraction
Alkylation
Vacuum distillation
Heavy vacuum
gas oil
Hydrocracking
Fuel oil
Vacuum
residue
Delayed coker
Hydrotreatment
Reforming
Coke
Gasoline blending pool
Gasoline,
naphtha

Figure 1

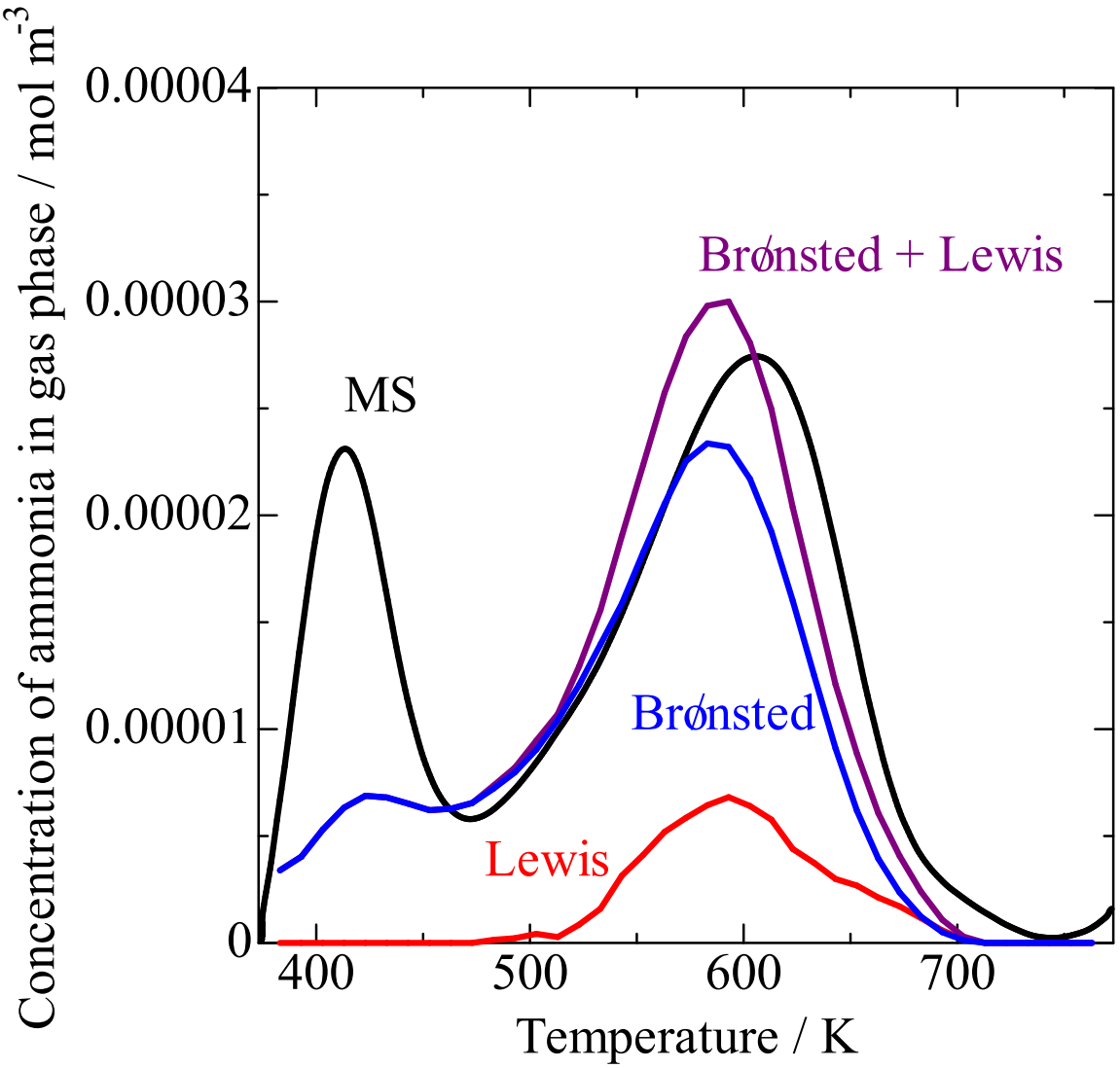
Concentration of ammonia in gas phase / mol m-3
0.00004
0.00003
0.00002
0.00001
0
400
500
600
700
Temperature / K
Brønsted + Lewis
MS
Brønsted
Lewis

Figure 2

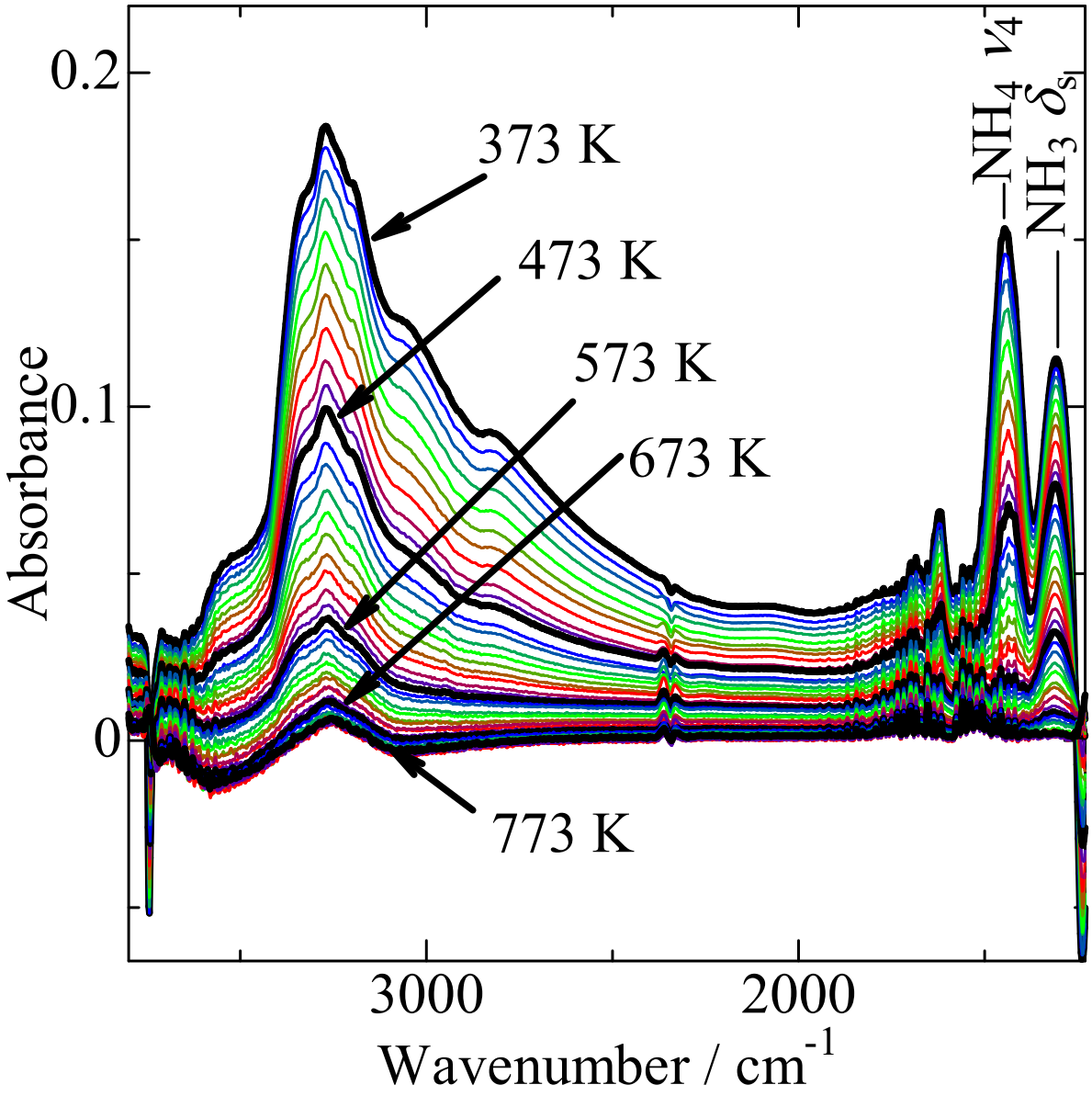
0.2
0.1
0
Absorbance
373 K
473 K
573 K
673 K
773 K
NH_4 ν_4
NH_3 δ_s
3000
2000
Wavenumber / cm^{-1}

Figure 3

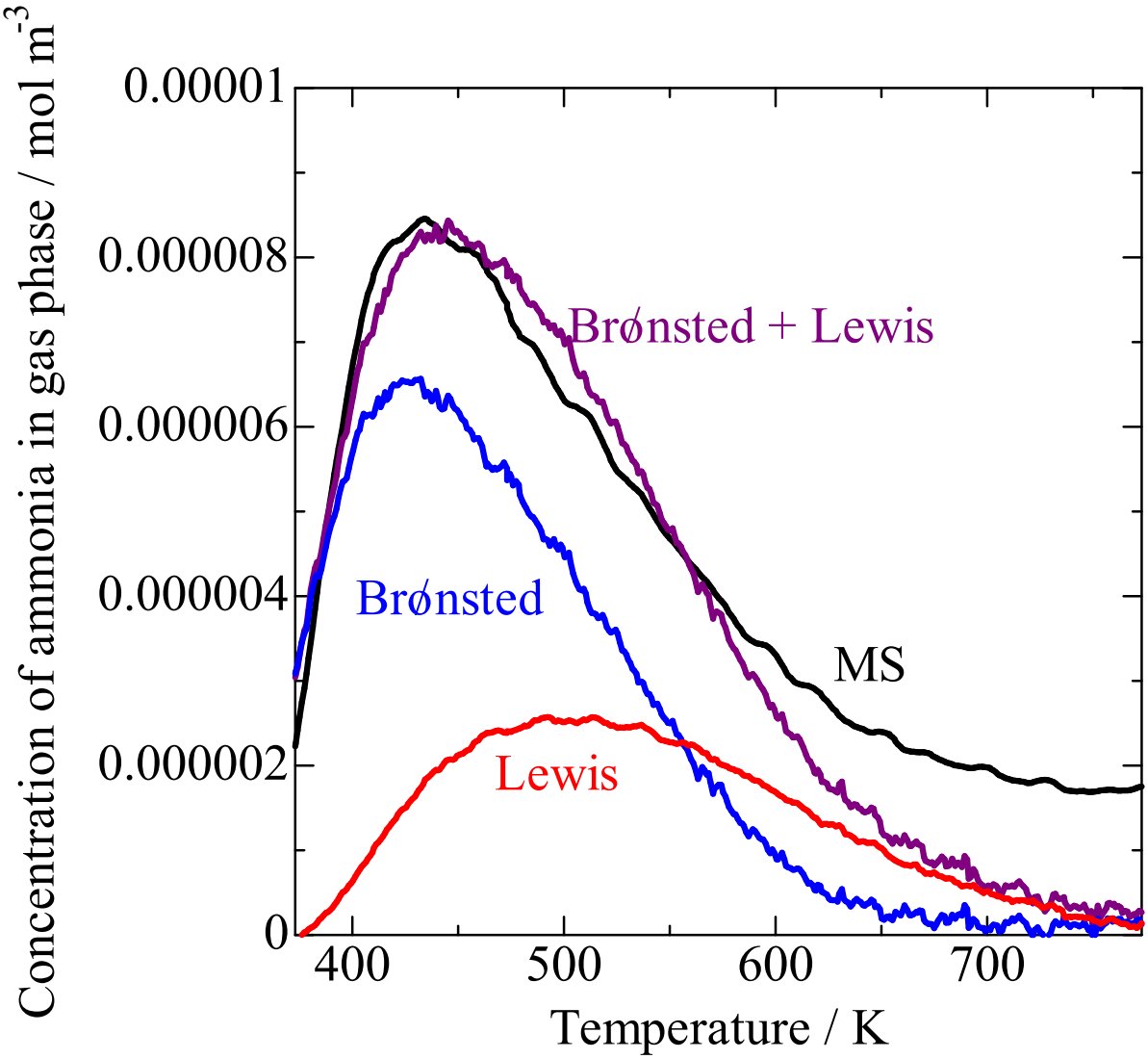
Concentration of ammonia in gas phase / mol m-3
0.00001
0.000008
0.000006
0.000004
0.000002
0
400
500
600
700
Temperature / K
Brønsted + Lewis
Brønsted
MS
Lewis

Figure 4

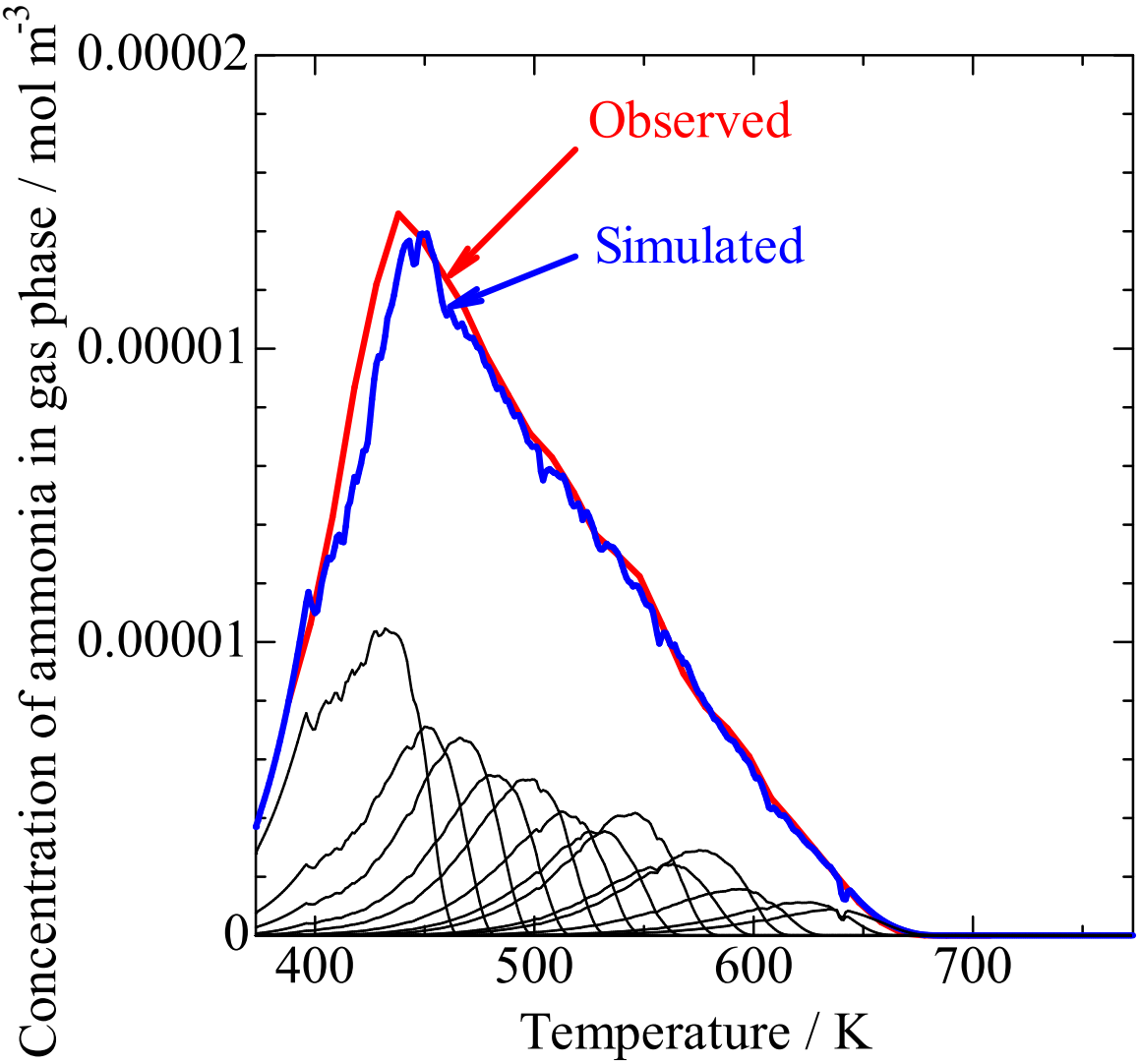
Concentration of ammonia in gas phase / mol m-3
0.00002
0.00001
0.00001
0
Observed
Simulated
400
500
600
700
Temperature / K

Figure 5

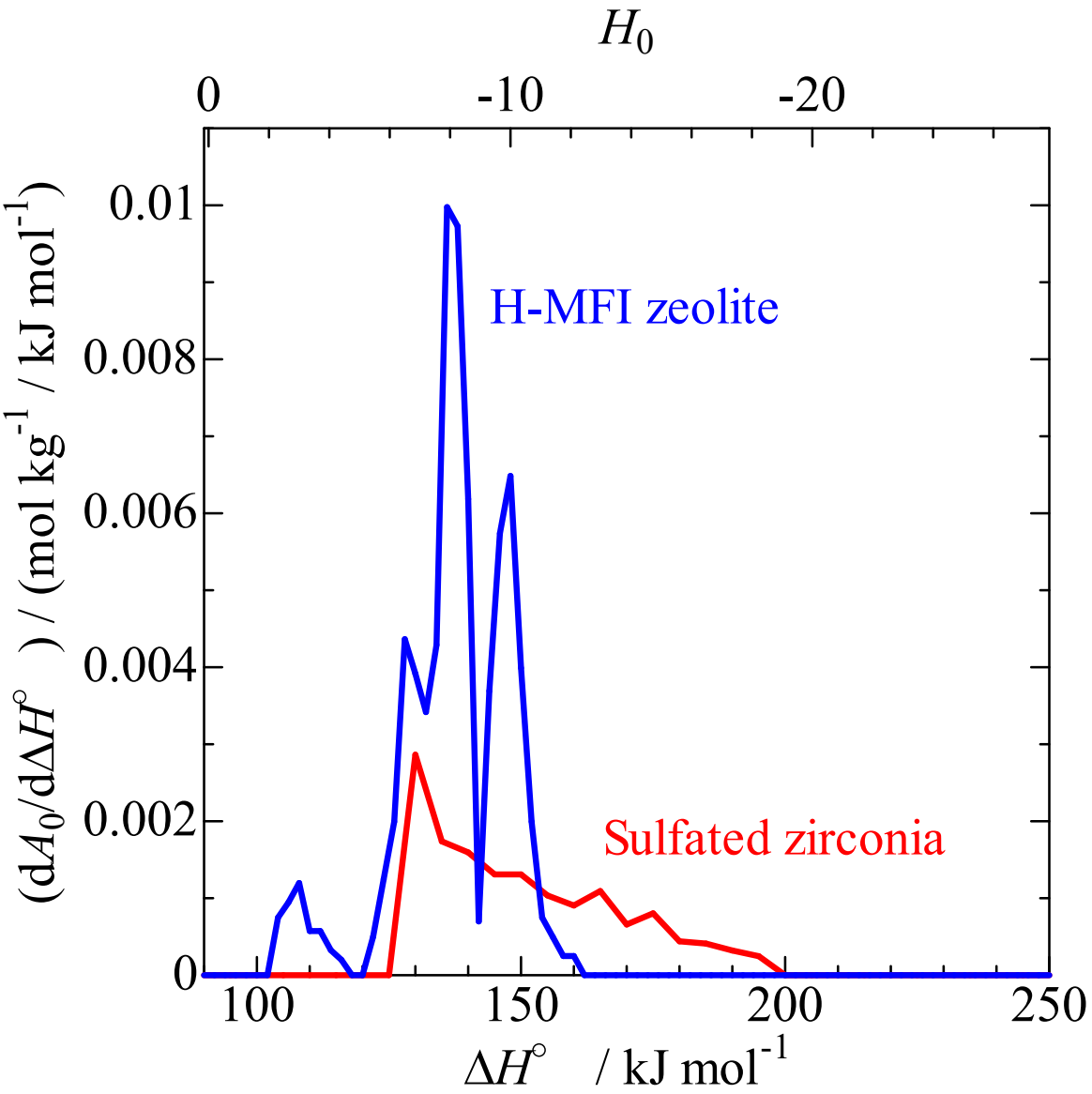
H_0
0
-10
-20
0.01
0.008
0.006
0.004
0.002
0
$(dA_0/d\Delta H^\circ)$ / (mol kg^{-1} / kJ mol^{-1})
H-MFI zeolite
Sulfated zirconia
100
150
200
250
ΔH° / kJ mol^{-1}

Figure 6

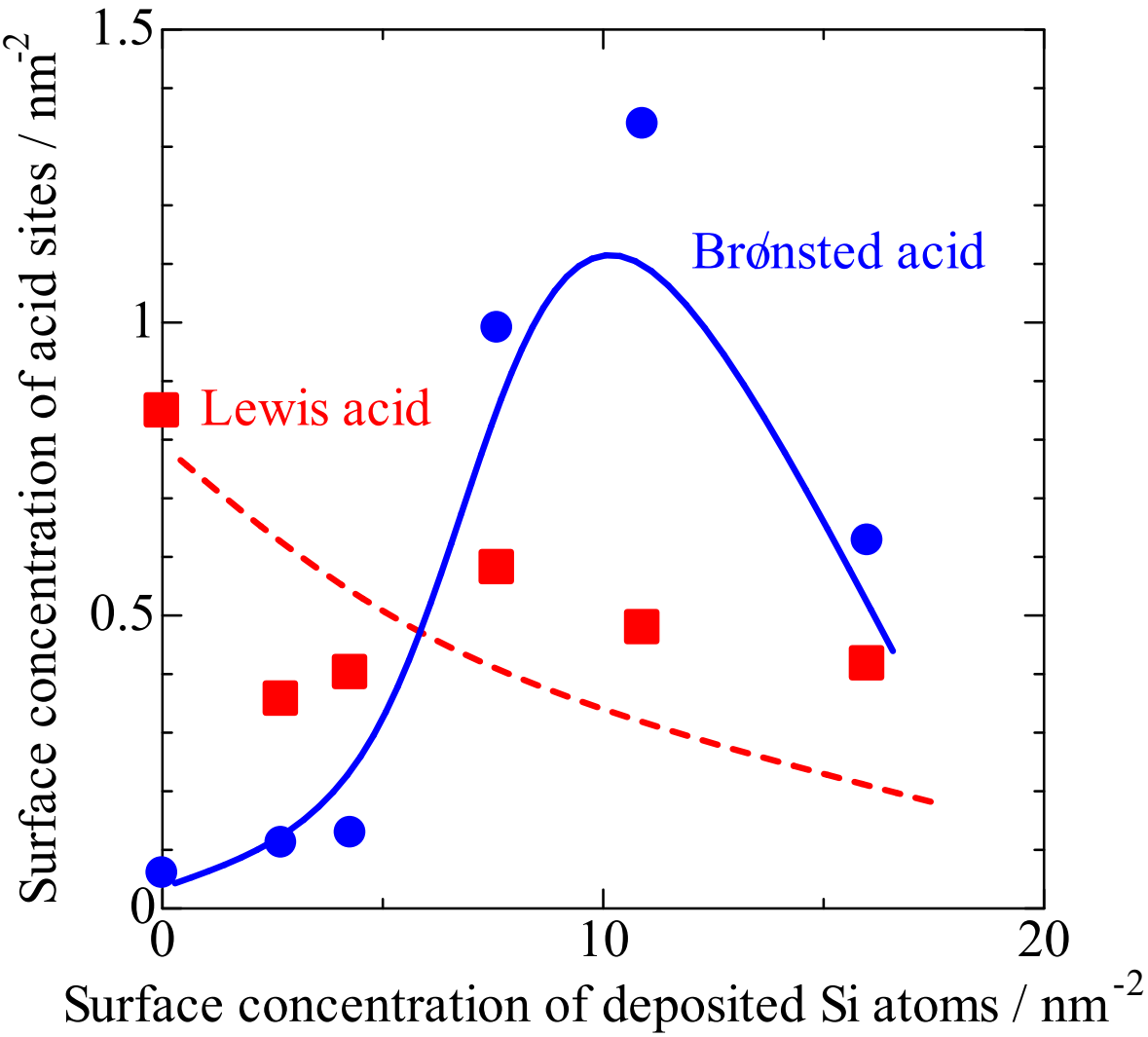
Surface concentration of acid sites / nm-2
1.5
1
0.5
0
Brønsted acid
Lewis acid
0
10
20
Surface concentration of deposited Si atoms / nm-2

Figure 7

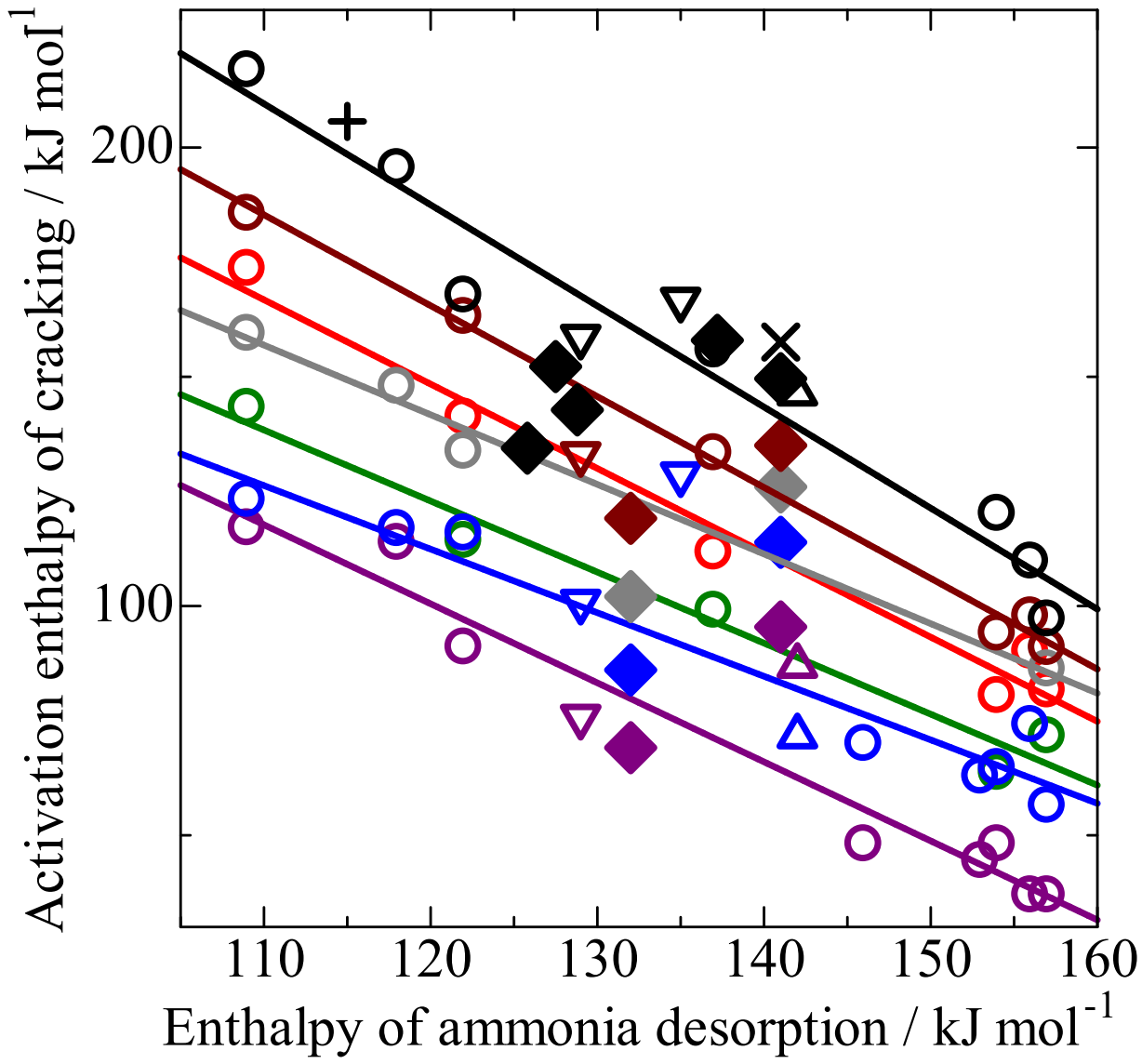
Activation enthalpy of cracking / kJ mol-1
200
100
110
120
130
140
150
160
Enthalpy of ammonia desorption / kJ mol-1

Figure 8

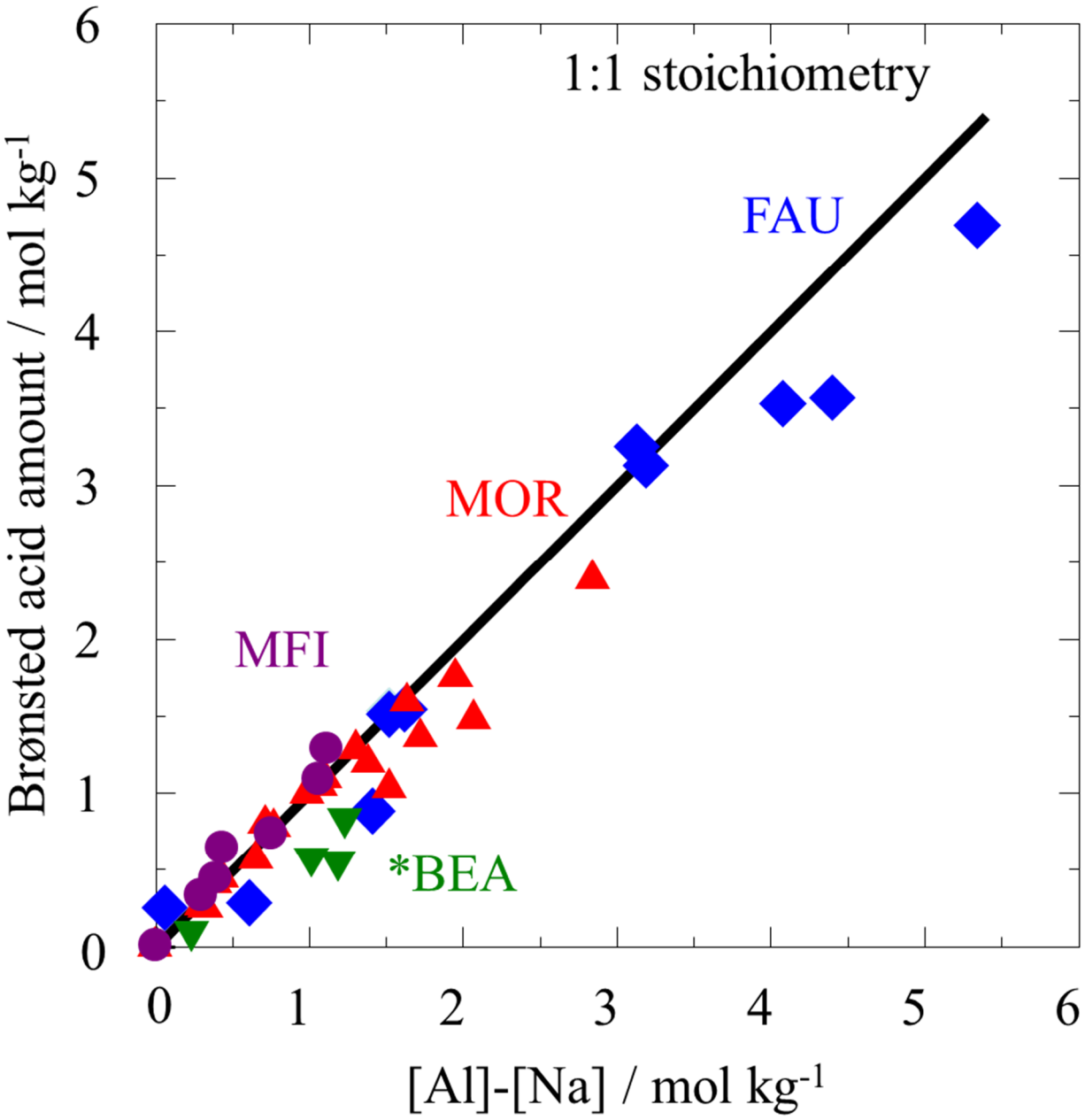
1:1 stoichiometry
FAU
MOR
MFI
*BEA
Brønsted acid amount / mol kg-1
[Al]-[Na] / mol kg-1
0
1
2
3
4
5
6

Figure 9

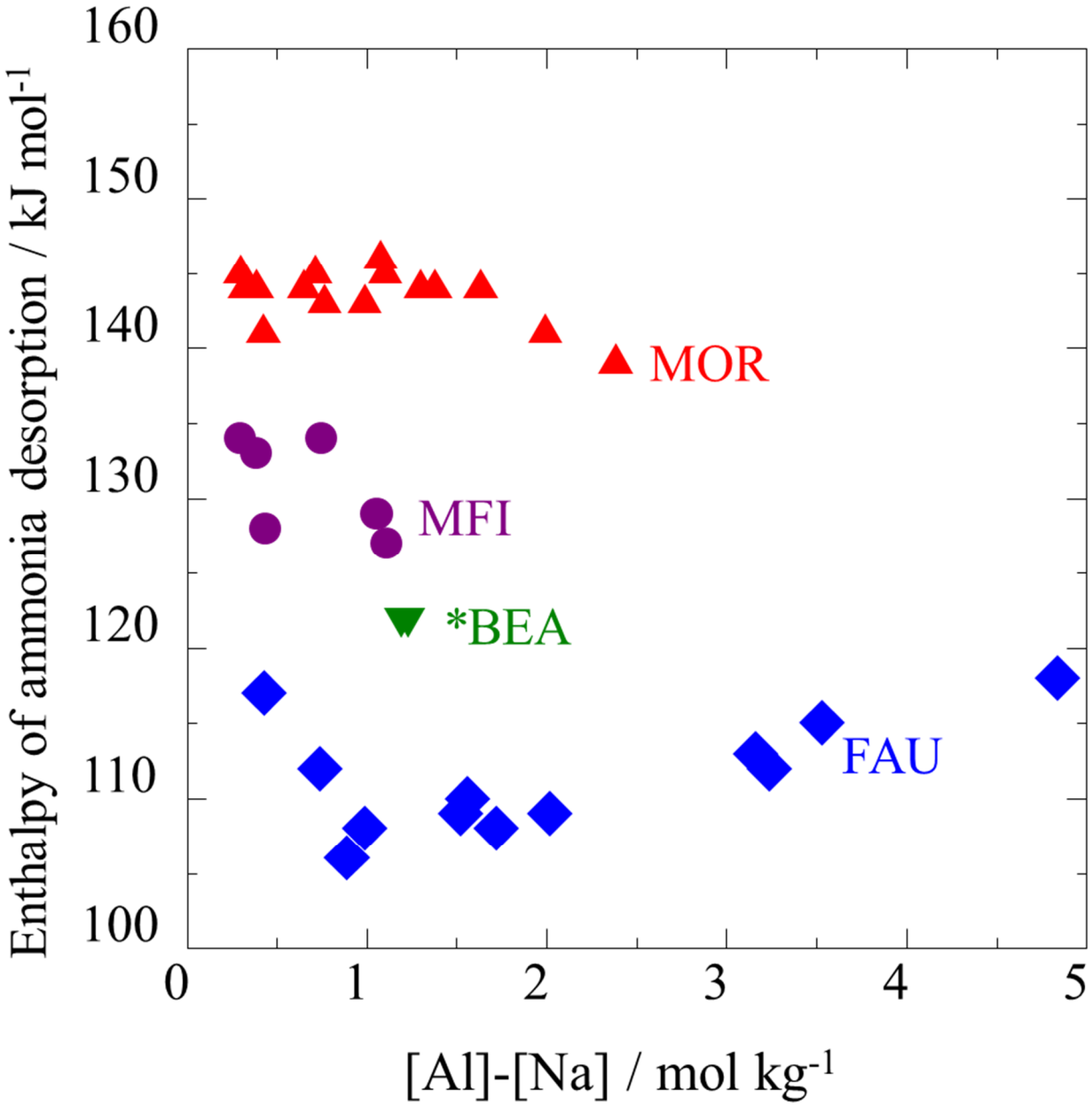
160
150
140
130
120
110
100
0
1
2
3
4
5
Enthalpy of ammonia desorption / kJ mol-1
[Al]-[Na] / mol kg-1
MOR
MFI
*BEA
FAU

Figure 10

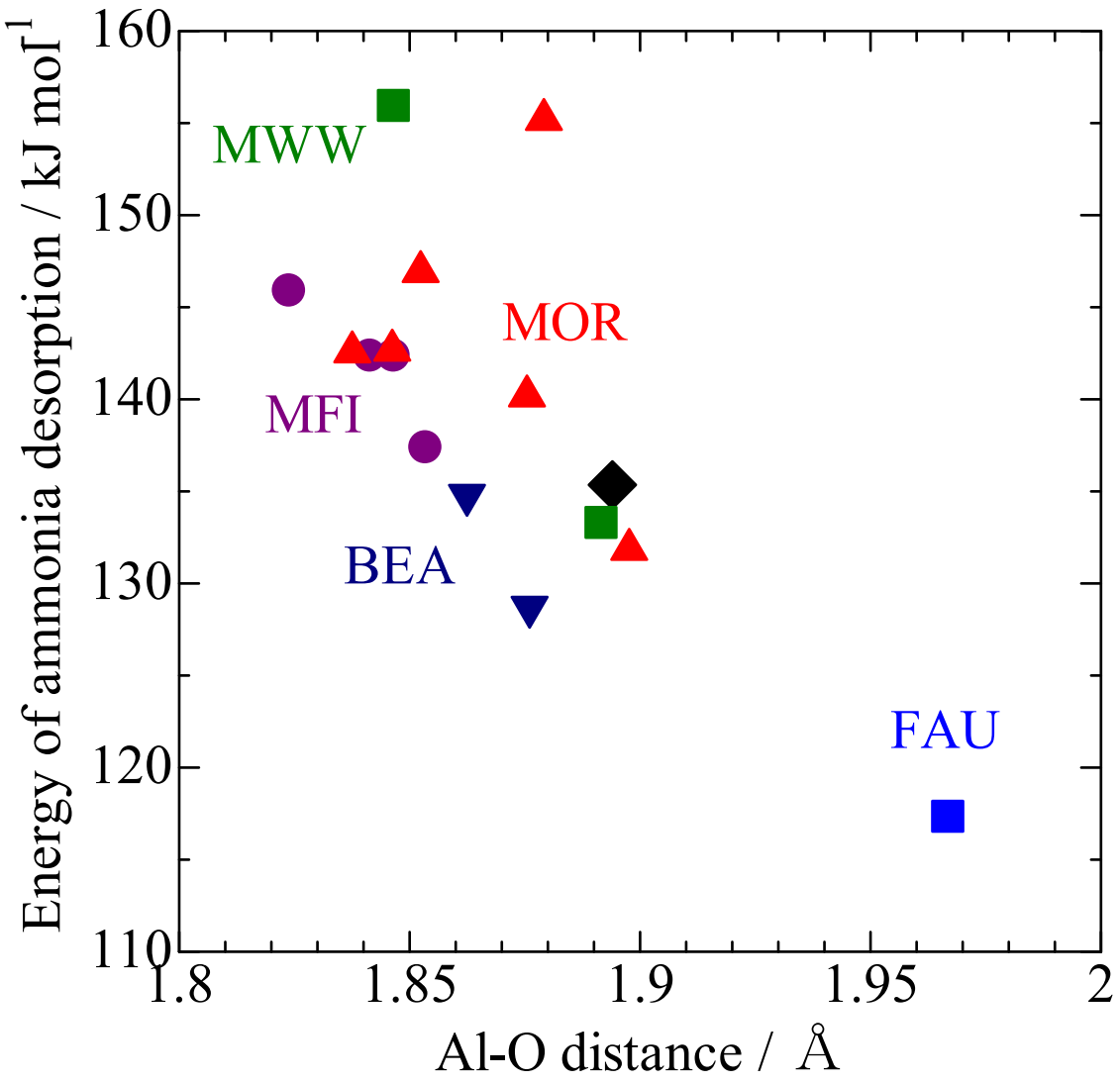
Energy of ammonia desorption / kJ mol-1
160
150
140
130
120
110
1.8
1.85
1.9
1.95
2
Al-O distance / Å
MWW
MOR
MFI
BEA
FAU

Figure 11

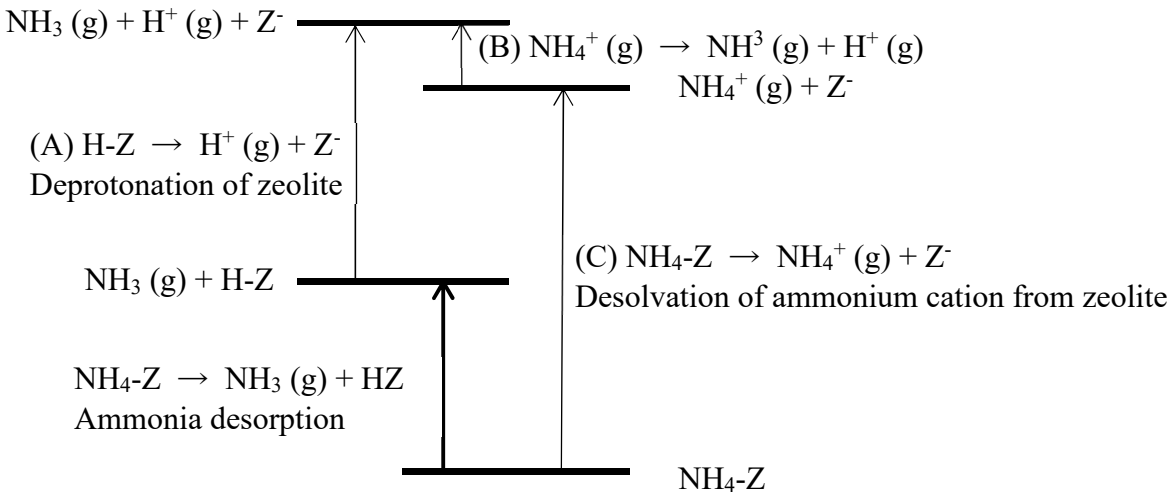
NH3 (g) + H+ (g) + Z-
(B) NH4+ (g) → NH3 (g) + H+ (g)
NH4+ (g) + Z-
(A) H-Z → H+ (g) + Z-
Deprotonation of zeolite
(C) NH4-Z → NH4+ (g) + Z-
Desolvation of ammonium cation from zeolite
NH3 (g) + H-Z
NH4-Z → NH3 (g) + HZ
Ammonia desorption
NH4-Z

Figure 12